

Neutrino-Dominated Accretion and Supernovae

Kazunori Kohri^{†,*}

Ramesh Narayan[†]

Tsvi Piran^{**,‡}

[†]*Harvard-Smithsonian Center for Astrophysics, 60 Garden Street, Cambridge, MA 02138*

^{*}*Department of Earth and Space Science, Osaka University, Toyonaka 560-0043, Japan*

^{**}*Racah Institute for Physics, Hebrew University, Jerusalem 91904, Israel*

[‡]*Theoretical Astrophysics Caltech, Pasadena, CA 91125, USA*

kkohri@cfa.harvard.edu

ABSTRACT

We suggest that part of the infalling material during the core-collapse of a massive star goes into orbit around the compact core to form a hot, dense, centrifugally-supported accretion disk whose evolution is strongly influenced by neutrino interactions. Under a wide range of conditions, this neutrino-dominated accretion flow will be advection-dominated and will develop a substantial out-flowing wind. We estimate the energy carried out in the wind and find that it exceeds 10^{50} erg for a wide range of parameters and even exceeds 10^{51} erg for reasonable parameter choices. We propose that the wind energy will revive a stalled shock and will help produce a successful supernova explosion. We discuss the role of the disk wind in both prompt and delayed explosions. While both scenarios are feasible, we suggest that a delayed explosion is more likely, and perhaps even unavoidable. Finally, we suggest that the disk wind may be a natural site for r -process nucleosynthesis.

Subject headings: accretion, accretion disks — black hole physics — neutrinos — supernovae : general

1. Introduction

Almost forty years after the original computations of Colgate & White (1966) and Arnett (1967), it is still not known exactly how core collapse supernovae explode. Quite early on it

became clear that the prompt shock that follows the bounce of the core stagnates, leading to a standing shock at a distance of several hundred km from the center. The region interior to the shock contains hot material that settles onto the central core, while the exterior contains infalling matter. Unless some additional energy source is available to energize the post-shock gas, the shock will ultimately run out of energy and we would have a failed explosion.

During the mid eighties, Wilson (1985) and Bethe & Wilson (1985; see also Goodman, Dar & Nussinov 1987) suggested that late time neutrino heating, about a second after the bounce, could lead to a revival of the shock and to ejection of the infalling envelope. However, later calculations indicated that this late neutrino heating might be insufficient. The fact that the explosion energy (a few foe $\equiv 10^{51}$ erg) is much smaller than the binding energy of the neutron star (a few hundred foe) gave some hope that small details in the calculations may change the result, leaving open the possibility that yet more sophisticated calculations might ultimately produce an explosion. However, recent detailed computations, carried out by different groups with improved neutrino transport and fully relativistic hydrodynamics (Bruenn 1985; Bruenn & Mezzacappa 1997; Bruenn, De Nisco, & Mezzacappa 2001; Liebendorfer et al. 2001, 2004; Mezzacappa, et al. 2001; Myra & Burrows, 1990; Rampp & Janka 2000; Thompson, Burrows & Pinto 2003), have demonstrated conclusively that one-dimensional, i.e., spherically-symmetric, simulations do not lead to a supernova (see Burrows & Thompson, 2002 for a recent review). A consensus has emerged that the coupling efficiency of the emerging neutrinos to the mantle is too small to lead to an explosion, so that the failure to explode is not an artifact of inaccurate calculations. The neutrinos simply do not transfer enough energy to the mantle, and something else is required beyond one-dimensional collapse and neutrino transport (see e.g. Burrows & Thompson, 2002).

Two-dimensional calculations carried out in the mid nineties (Herant et al. 1994; Burrows, Hayes & Fryxell, 1995; Janka & Muller, 1996; Fryer et al. 1999) resulted in successful supernovae. These calculations also revealed turbulence in the collapsing gas, and it was suggested that the explosion was the result of an enhancement of the coupling between the neutrinos and the mantle due to the turbulence (Burrows & Thompson, 2002). However, it is unclear at present whether or not the results are an artifact of the simplified transport models used in the simulations. It is also unclear if the two-dimensional turbulence seen in the calculations provides a realistic description of full three-dimensional turbulence (see e.g., Fryer & Warren 2002, 2004).

In view of this confusing situation, it would be wise to search for additional energy sources that might transport energy to the mantle and lead to an explosion. Burrows & Goshy (1993) describe the explosion problem in terms of the neutrino luminosity needed to produce an explosion at a given mass accretion rate. Clearly, what is important is the

energy flux, whether it is via neutrinos or something else. In fact, energy in a form other than neutrinos is likely to be superior since it might couple more efficiently to the matter in the mantle¹.

Two energy sources that have been mentioned a number of times in connection with the supernova problem are magnetic fields (Le Blanc & Wilson, 1970; Moiseenko, Bisnovatyi-Kogan & Ardeljan 2004; Kotake et al. 2004; Wheeler, Meier & Wilson 2002) and rotation. Rotation has been discussed as the cause of asymmetry in the explosion and also in the context of generating gravitational waves. Recent progress in numerical computations have enabled modeling rotating collapse with a realistic equation of state and neutrino transport in two dimensions (Fryer & Heger 2000; Kotake, Yamada & Sato 2003; Livne et al., 2004; Walder et al. 2004; and references therein) and even three dimensions (Fryer & Warren 2004; Janka et al. 2004). Some of these studies indicate that rotation may cause a weakening of two-dimensional convection and thereby delay the explosion (Fryer & Heger, 2000). However, more work is needed before one can be sure of the net effect of rotation on supernova explosions.

We discuss in this paper a novel scenario, based on rotation, which does not seem to have been considered before. We suggest that a core-collapse supernova may be partially driven by wind energy from an accretion disk that forms around the proto-neutron star (inside the stalled shock). Such a disk is expected to form if the pre-explosion stellar core rotates reasonably rapidly. The required progenitor rotation rate for our scenario to work is comparable to, or perhaps even larger than, the rates predicted in current stellar evolution models (e.g., Heger et al. 2000, 2004). However, there are large uncertainties in the stellar model calculations.

In our model, because of the high angular momentum of the stellar gas, the infalling matter arranges itself into a dense and very hot disk in the form of a Neutrino Dominated Accretion Flow (NDAF; Popham, Woosley & Fryer 1999; Narayan, Piran & Kumar 2001; Kohri & Mineshige 2002; Di Matteo, Perna & Narayan 2002)². For a wide range of parameter space, an NDAF is advection-dominated and is expected to emit a substantial wind. We propose that the mechanical energy transported out by this wind will be transferred to

¹The efficiency of capturing neutrinos is usually considered to be less than a percent. But this is the ratio of the neutrinos captured to the total number of neutrinos radiated. However, the neutrino emission lasts for ten seconds while the delayed shock phase lasts only one second. What is more relevant for our comparison is the capture efficiency of a few percent that corresponds to the ratio of neutrinos captured to the neutrinos radiated during the delayed shock phase — a few $\times 10^{52}$ erg (Burrows & Thompson 2002).

²For a numerical simulation of the dynamical evolution of an NDAF, see Lee, Ramirez-Ruiz & Page (2004).

the gas inside the stalled shock, reviving the shock and leading to a successful explosion. Related ideas have been discussed by MacFadyen (2003) and Thompson, Quataert & Burrows (2004). Note that the wind that we consider originates from the disk and is different from the spherical wind originating from the proto-neutron star itself discussed by Thompson et al. (2000).

§ 2 of the paper presents a detailed discussion of the structure of the NDAF that forms during core collapse. The model we employ for the calculations is more elaborate than those described in the recent literature (Popham et al. 1999; Narayan et al. 2001; Kohri & Mineshige 2002; Di Matteo et al. 2002), and we highlight the improvements. Some of the relevant physics is described in Appendices A and B. These structure equations are applicable to an NDAF residing in the core of a collapsar (MacFadyen & Woosley 1999) and may be of use for numerical simulations of collapsars. The reader who is not interested in the technical details and wishes to read about the application to supernovae is invited to skip § 2 and to go directly to § 3, where we calculate the mechanical energy that is likely to be carried in the disk wind. Even with fairly conservative assumptions, we show that up to about 10^{51} erg of energy might be available in the wind. We suggest that this energy would help to energize the stalled post-bounce shock in a supernova. The material in the wind may also participate in r -process nucleosynthesis. § 4 concludes with a discussion.

2. Model of a Neutrino Dominated Accretion Disk

2.1. Physical variables

In this paper we use the following dimensionless variables for the mass of the compact star M , the accretion rate \dot{M} and the radius R :

$$m \equiv M/M_{\odot}, \quad (1)$$

$$\dot{m} \equiv \dot{M}/(M_{\odot} \text{ s}^{-1}), \quad (2)$$

$$r \equiv R/R_{\text{S}} = R/(2.95 \times 10^5 m \text{ cm}), \quad (3)$$

where R_{S} is the Schwarzschild radius.

We also scale the matter density ρ and the temperature T as follows:

$$\rho_{10} \equiv \rho/(10^{10} \text{ g cm}^{-3}), \quad (4)$$

$$T_{11} \equiv T/(10^{11}\text{K}). \quad (5)$$

We write the surface density of the disk as

$$\Sigma = 2H\rho, \quad (6)$$

where the disk half-thickness (or disk height) H is given by

$$H = c_S/\Omega_K. \quad (7)$$

Here c_S is the sound speed, which is defined by

$$c_S = \sqrt{p/\rho}, \quad (8)$$

and Ω_K the Keplerian angular velocity, given by

$$\Omega_K = \sqrt{GM/R^3} = 17.19 \times 10^4 m^{-1} r^{3/2} \text{ s}^{-1}. \quad (9)$$

The pressure p is the sum of contributions from radiation, electrons/positrons, nuclei, and neutrinos:

$$p = p_{\text{rad}} + p_e + p_{\text{gas}} + p_\nu \quad (10)$$

In the next subsection, we discuss each component of the pressure in detail.

2.2. Contributions to the Pressure

The radiation pressure is given by

$$p_{\text{rad}} = \frac{1}{3}aT^4 = 2.52 \times 10^{29} \text{ erg cm}^{-3} T_{11}^4, \quad (11)$$

where a is the radiation density constant. The gas pressure (from nuclei) is

$$p_{\text{gas}} = \rho k_B T / m_N = 3.26 \times 10^{28} \text{ erg cm}^{-3} \rho_{10} T_{11}, \quad (12)$$

where m_N is the mean mass of nuclei. We are mostly interested in fully dissociated nuclei, so m_N is the mass of a nucleon, where we ignore the mass difference between a proton and a neutron.

For the electron pressure, it is important to consider a general form that is valid even when electrons are degenerate and/or relativistic. We write

$$p_e = p_{e^-} + p_{e^+}, \quad (13)$$

where the two terms represent the contributions from electrons and positrons, given by

$$p_{e^-} = \frac{1}{3\pi^2\hbar^3c^3} \int_0^\infty dp \frac{p^4}{\sqrt{p^2c^2 + m_e^2c^4}} \frac{1}{e^{(\sqrt{p^2c^2 + m_e^2c^4} - \mu_e)/k_B T} + 1}, \quad (14)$$

$$p_{e^+} = \frac{1}{3\pi^2\hbar^3c^3} \int_0^\infty dp \frac{p^4}{\sqrt{p^2c^2 + m_e^2c^4}} \frac{1}{e^{(\sqrt{p^2c^2 + m_e^2c^4} + \mu_e)/k_B T} + 1}, \quad (15)$$

μ_e is the chemical potential of electrons, c is the speed of light, and m_e is the electron mass. Note that the above expression is applicable for both relativistic and nonrelativistic electrons. The chemical potential μ_e has to be determined self-consistently, as we discuss in detail in the next two subsections. In Fig. 1 (a), we show contours of p_e in units of erg cm^{-3} in the T – η_e plane, where η_e is the degeneracy parameter of electrons, defined by

$$\eta_e = \mu_e/(k_B T). \quad (16)$$

This parameter is a good measure of the electron degeneracy. If η_e is much larger than unity, the electrons are strongly degenerate, whereas, if $\eta_e \ll 1$, the electrons are weakly degenerate and we can ignore degeneracy.

The last term in Eq. (10) is the pressure of the neutrinos, $p_\nu = \sum_{i=e,\mu,\tau} p_{\nu_i}$, for the three species $\nu_i = \nu_e, \nu_\mu, \nu_\tau$. Adopting the approximate formula in Popham & Narayan (1995) and Di Matteo, Perna & Narayan (2002), we write

$$\begin{aligned} p_{\nu_i} &= \frac{1}{3} u_{\nu_i} = \frac{1}{3} \frac{(7/8)aT^4 (\tau_{\nu_i}/2 + 1/\sqrt{3})}{\tau_{\nu_i}/2 + 1/\sqrt{3} + 1/(3\tau_{a,\nu_i})} \\ &= 2.21 \times 10^{29} \text{ erg cm}^{-3} T_{11}^4 \frac{\tau_{\nu_i}/2 + 1/\sqrt{3}}{\tau_{\nu_i}/2 + 1/\sqrt{3} + 1/(3\tau_{a,\nu_i})}. \end{aligned} \quad (17)$$

The various neutrino “optical depths” τ are discussed in detail in subsection 2.3.3 (see, Eqs. (55), (56) and (57)).

2.2.1. Chemical potential of electrons

When electrons are degenerate, some important effects are introduced. First, the process of neutrino emission is considerably modified; for example, pair creation of neutrinos and antineutrinos is suppressed because of the asymmetry between electrons and positrons. In addition, as we have discussed above, the expression for the electron pressure is modified.

The asymmetry between electrons and positrons is characterized by the electron chemical potential μ_e , which is determined by the condition of charge neutrality among protons,

electrons and positrons. Let us introduce the net number density of electrons n_e . Charge neutrality requires

$$n_e \equiv n_{e^-} - n_{e^+} = n_p, \quad (18)$$

where n_p is the number density of protons. The number densities of electrons and positrons are given by

$$n_{e^-} = \frac{1}{\hbar^3 \pi^2} \int_0^\infty dp p^2 \frac{1}{e^{(\sqrt{p^2 c^2 + m_e^2 c^4} - \mu_e)/k_B T} + 1}, \quad (19)$$

$$n_{e^+} = \frac{1}{\hbar^3 \pi^2} \int_0^\infty dp p^2 \frac{1}{e^{(\sqrt{p^2 c^2 + m_e^2 c^4} + \mu_e)/k_B T} + 1}. \quad (20)$$

Thus, for given n_p and T , we can solve equation (18) to obtain μ_e , and thereby calculate n_{e^-} and n_{e^+} . We plot contours of n_e in the T – η_e plane in Fig. 1 (b).

2.2.2. Neutron to proton ratio

To calculate the chemical potential μ_e for a given matter density ρ and temperature T , we should know the correct value of *the neutron to proton ratio*, $n/p \equiv n_n/n_p$, since this determines the value of n_p needed in equation (18). Here n_N ($N = n, p$) is the number density of nucleon N . We need n/p also to calculate the neutrino emission rates in § 2.3.3. Therefore, it is quite crucial to obtain n/p as accurately as possible. We briefly discuss here the procedure we employ, leaving the details to Appendix B.

To obtain n/p , we need to solve a set of reaction equations between neutrons and protons. We consider only the weak interaction; since the mean energy of nucleons in the system is much lower than the rest mass energy of pions $m_\pi c^2 \sim 140$ MeV, we may ignore the strong interaction. We assume that the photons and electrons (including positrons) are completely thermalized since the timescale of electromagnetic interactions is much shorter than the dynamical timescale (see Appendix A). The reaction equations between protons and neutrons are then given by

$$\frac{dn_p}{dt} = -\Gamma_{p \rightarrow n} n_p + \Gamma_{n \rightarrow p} n_n, \quad (21)$$

$$\frac{dn_n}{dt} = +\Gamma_{p \rightarrow n} n_p - \Gamma_{n \rightarrow p} n_n, \quad (22)$$

where $\Gamma_{p \rightarrow n}$ ($\Gamma_{n \rightarrow p}$) is the transition rate from proton to neutron (neutron to proton). The rate is represented by the sum of several weak interaction rates: $\Gamma_{p \rightarrow n} = \Gamma_{pe^- \rightarrow n \nu_e} + \Gamma_{p \bar{\nu}_e \rightarrow n e^+} +$

$\Gamma_{pe^-\bar{\nu}_e \rightarrow n}$ ($\Gamma_{n \rightarrow p} = \Gamma_{ne^+ \rightarrow p\bar{\nu}_e} + \Gamma_{n\nu_e \rightarrow pe^-} + \Gamma_{n \rightarrow pe^-\bar{\nu}_e}$), with

$$\Gamma_{ne^+ \rightarrow p\bar{\nu}_e} = K_1 \int_{Q/c+m_e c}^{\infty} dp \left[\sqrt{(pc-Q)^2 - m_e^2 c^4} (pc-Q) \frac{p^2}{e^{(pc-Q+\mu_e)/k_B T} + 1} (1 - f_{\bar{\nu}_e}(p)) \right], \quad (23)$$

$$\Gamma_{pe^- \rightarrow n\nu_e} = K_1 \int_0^{\infty} dp \left[\sqrt{(pc+Q)^2 - m_e^2 c^4} (Q+pc) \frac{p^2}{e^{(pc+Q-\mu_e)/k_B T} + 1} (1 - f_{\nu_e}(p)) \right], \quad (24)$$

$$\Gamma_{n \rightarrow pe^-\bar{\nu}_e} = K_1 \int_0^{Q/c-m_e c} dp \left[\sqrt{(pc-Q)^2 - m_e^2 c^4} (Q-pc) \frac{p^2}{1 + e^{(pc-Q+\mu_e)/k_B T}} (1 - f_{\bar{\nu}_e}(p)) \right], \quad (25)$$

$$\Gamma_{n\nu_e \rightarrow pe^-} = K_1 \int_0^{\infty} dp \left[\sqrt{(pc+Q)^2 - m_e^2 c^4} (pc+Q) \frac{p^2}{1 + e^{-(pc+Q-\mu_e)/k_B T}} f_{\nu_e}(p) \right], \quad (26)$$

$$\Gamma_{pe^-\bar{\nu}_e \rightarrow n} = K_1 \int_0^{Q/c-m_e c} dp \left[\sqrt{(pc-Q)^2 - m_e^2 c^4} (Q-pc) \frac{p^2}{e^{-(pc-Q+\mu_e)/k_B T} + 1} f_{\bar{\nu}_e}(p) \right], \quad (27)$$

$$\Gamma_{p\bar{\nu}_e \rightarrow ne^+} = K_1 \int_{Q/c+m_e c}^{\infty} dp \left[\sqrt{(pc-Q)^2 - m_e^2 c^4} (Q-pc) \frac{p^2}{1 + e^{-(pc-Q+\mu_e)/k_B T}} f_{\bar{\nu}_e}(p) \right], \quad (28)$$

where f_{ν_e} ($f_{\bar{\nu}_e}$) is the distribution function of electron neutrinos (antineutrinos), and $Q = (m_n - m_p)c^2 = 1.29$ MeV. The normalization factor K_1 is obtained from the neutron lifetime τ_n as $K_1 = G_F^2(1+3g_A)c/(2\pi^3\hbar^3) \simeq (1.636\tau_n)^{-1}$, where G_F is the Fermi coupling constant and g_A is the axial vector coupling constant. The present best estimate of the neutron lifetime is $\tau_n \simeq 885.7 \pm 0.8$, according to a recent compilation of the experimental data (Eidelman et al. 2004). For reference, we plot the timescale of $\Gamma_{pe^- \rightarrow n\nu_e}^{-1}$ and $\Gamma_{ne^+ \rightarrow p\bar{\nu}_e}^{-1}$ in the T - η_e plane in Fig. 2 (a) and Fig. 2 (b), respectively. These are the two most important rates for the calculation of n/p (see the discussion in Appendix B).

The equilibrium value of the neutron to proton ratio is calculated by imposing the condition $dn_p/dt = dn_n/dt = 0$. From Eqs. (21) and (22), this gives

$$\left(\frac{n}{p}\right) = \frac{\Gamma_{p \rightarrow n}}{\Gamma_{n \rightarrow p}}. \quad (29)$$

Note that the electron chemical potential μ_e is implicitly present in the above relation since the interconverting reaction rates all depend on it. On the other hand, the solution for μ_e via the charge neutrality condition Eq. (18) requires the value of n/p . Thus we have a highly nonlinear coupled system of equations which has to be solved recursively, given the matter density ρ and the temperature T .

To calculate n/p via Eq. (29), we need to know the distribution function of neutrinos f_{ν_e} and antineutrinos $f_{\bar{\nu}_e}$. If the neutrinos are perfectly thermalized and have an ideal Fermi-Dirac distribution, then from Eq. (29) with Eqs. (23) – (28) we obtain a simple analytic

expression for the neutron to proton ratio,

$$\left(\frac{n}{p}\right)_{\text{Eq}} = \exp\left(-\frac{Q}{k_{\text{B}}T} + \eta_e\right). \quad (30)$$

But this result is valid only for perfect thermodynamic equilibrium³.

In the more general case, when the neutrinos are not fully thermalized, we have to calculate the correct form of the distribution function of neutrinos. The exact way to do this is to solve a set of Boltzmann equations for the time-evolution and energy transfer. This is a major exercise which is not necessary for our present purpose. We have instead adopted an approximate procedure, which is discussed in Appendix B.

2.3. Heating and cooling rates

2.3.1. Heating rate

In the theory of accretion disks, the energy balance between heating and cooling processes plays an important role. The standard thin accretion disk solution corresponds to the case in which energy loss by cooling dominates over energy advection, whereas an advection-dominated accretion flow corresponds to the opposite limit (Narayan & Yi 1994, 1995a).

Making use of the standard disk equations (e.g., Frank, King & Raine 1992), the vertically integrated viscous heating rate (per unit area) over a half thickness H is given by

$$Q^+ = Q_{\text{vis}}^+ = \frac{3}{8\pi} G \frac{M\dot{M}}{R^3} = 1.23 \times 10^{42} \text{ m}^{-2} \dot{m} r^3 \text{ erg cm}^{-2} \text{ s}^{-1}. \quad (31)$$

The mass accretion rate \dot{M} can be written in terms of the viscosity coefficient ν as

$$\dot{M} = 4\pi\rho R H v_r \approx 6\pi\nu\rho H, \quad (32)$$

³For simplicity, we have ignored the chemical potential of neutrinos. This approximation is reasonable for our problem because the region where the neutrinosphere appears is immediately replaced by fresh plasma from the outer optically thin region (but nucleons are still in beta equilibrium) until a large amount of lepton asymmetry is produced in the disk. In the optically thick region, the timescale for order unity change of the electron neutrino chemical potential by neutrino emission is typically ~ 1 sec. In comparison, the viscous timescale R/v_r and the dynamical timescale $1/\Omega$ of the accreting matter are less than 0.1 sec (see § 3). Note that this is different from the normal case of spherical collapse in a supernova. Incidentally, note also that Eq. (30) is not the observed neutrino spectrum from the SN; it is the local neutrino distribution. It is well-known that the observed spectrum is modified from the perfect Fermi-Dirac distribution by the energy dependence of the cross section of neutrino-nucleon reactions. Usually, this is fitted by using the effective chemical potential of the neutrino.

where v_r is the radial velocity of the gas. For the viscosity, we use the standard α prescription,

$$\nu = \alpha c_S^2 / \Omega_K = 0.1 \alpha_{-1} c_S^2 / \Omega_K, \quad \alpha_{-1} \equiv \alpha / 0.1. \quad (33)$$

For simplicity, we have ignored a boundary correction term in Eq. (32) (see Frank et al. 1992).

2.3.2. Cooling rate

The rate of loss of energy by cooling has four contributions:

$$Q^- = Q_{\text{rad}}^- + Q_{\text{photodiss}}^- + Q_{\text{adv}}^- + Q_{\nu}^-, \quad (34)$$

where Q_{rad}^- is the radiative cooling rate, $Q_{\text{photodiss}}^-$ is the cooling rate by photodissociation of heavy nuclei, Q_{adv}^- is the advective energy transport (Abramowicz et al. 1988; Narayan & Yi 1994), and Q_{ν}^- is the cooling rate due to neutrino loss.

The radiative cooling rate is expressed by

$$Q_{\text{rad}}^- = \frac{g_* \sigma_s T^4}{2\tau_{\text{tot}}}, \quad (35)$$

where $\sigma_s = \pi^2 k_B^4 / (60 \hbar^3 c^2)$ is the Stefan-Boltzmann constant and g_* is the number of degrees of freedom ($= 2$ for photons). The optical depth, τ_{tot} , is given by

$$\tau_{\text{tot}} = \kappa_R \rho H = \frac{\kappa_R \Sigma}{2}, \quad (36)$$

where κ_R is the Rosseland-mean opacity,

$$\kappa_R = 0.40 + 0.64 \times 10^{23} \left(\frac{\rho}{\text{g cm}^{-3}} \right) \left(\frac{T}{\text{K}} \right)^{-3} \text{ g}^{-1} \text{ cm}^2. \quad (37)$$

The first term on the right is from electron scattering and the second is from free-free absorption. The radiative optical depth in an NDAF is extremely large; therefore, radiative cooling is negligible compared to the other cooling terms described below (i.e., the flow is extremely advection-dominated as far as the radiation is concerned).

Since the photodissociation of heavy nuclei requires energy, this process acts like a cooling mechanism. The cooling rate is given by

$$Q_{\text{photodiss}}^- = q_{\text{photodiss}}^- H, \quad (38)$$

with

$$q_{\text{photodiss}}^- = 6.8 \times 10^{28} \text{ erg cm}^{-3} \text{ s}^{-1} \rho_{10} \left(\frac{A}{4} \right)^{-1} \left(\frac{B}{28.3 \text{ MeV}} \right) \left(\frac{v_r}{\text{cm s}^{-1}} \right) \left(\frac{dX_{\text{nuc}}/dr}{\text{cm}^{-1}} \right), \quad (39)$$

where B is the binding energy of the nucleus ($=28.3$ MeV for ^4He), A is the mass number of the nucleus, and X_{nuc} is the mass fraction of nucleons, given by (Woosley & Baron 1992; Qian & Woosley 1996)

$$X_{\text{nuc}} = 295.5 \rho_{10}^{-3/4} T_{11}^{9/8} \exp(-0.8209/T_{11}). \quad (40)$$

In the context of an accretion disk, the radial velocity is (see Eq. (32))

$$v_r = \dot{M}/(2\pi R\Sigma) = 3\nu/(2R). \quad (41)$$

In Eq. (39), we have assumed that all the heavy nuclei are α 's. For other nuclei, we only need to change the binding energy B and the mass number A appropriately.

The advective cooling rate is given by (Kato, Fukue, & Mineshige 1998),

$$Q_{\text{adv}}^- = \Sigma T v_r \frac{ds}{dR}, \quad (42)$$

where s denotes the entropy per particle,

$$s = (s_{\text{rad}} + s_{\text{gas}}) / \rho. \quad (43)$$

Here, the entropy density of the radiation is

$$s_{\text{rad}} = \frac{2}{3} a g_* T^3, \quad (44)$$

and the entropy density of the gas (i.e., nonrelativistic particles) is

$$s_{\text{gas}} = \sum_i n_i \left(\frac{5}{2} + \ln \left[\frac{g_i}{n_i} \left(\frac{m_i T}{2\pi} \right)^{3/2} \right] \right), \quad (45)$$

where the suffix i runs over nonrelativistic nucleons and electrons, and g_i is the statistical degree of freedom of species i . Note that the entropy of degenerate particles is quite small. Therefore, we neglect it.

It is convenient to define an advection parameter f_{adv} (e.g., Narayan & Yi 1994),

$$f_{\text{adv}} = \frac{Q_{\text{adv}}^-}{Q^+} \approx \left(\frac{H}{R} \right)^2, \quad (46)$$

which measures the relative importance of advection.

2.3.3. Neutrino emission

Cooling by neutrino emission plays an important role in an NDAF and requires careful discussion. When the accreting gas is transparent to neutrinos, it is relatively straightforward to calculate the cooling rate (see Narayan, Piran & Kumar 2001; Kohri & Mineshige 2002). However, once the gas becomes opaque to neutrinos, the cooling rate is significantly modified. To handle this regime, we introduce the “optical depth” τ_{ν_i} for each neutrino species, $\nu_i = \nu_e, \nu_\mu$ or ν_τ , and follow the approach of Di Matteo, Perna & Narayan (2002) for estimating these optical depths.⁴

In the transparent limit, the total neutrino-cooling rate is simply the sum of four terms, $(q_{Ne}^- + q_{e^+e^-}^- + q_{\text{brems}}^- + q_{\text{plasmon}}^-)H$, where q_{Ne}^- is the cooling rate due to electron-positron capture by a nucleon “ N ” ($= p, n$), $q_{e^+e^-}^-$ is from electron-positron pair annihilation into neutrinos, q_{brems}^- is the cooling rate by nucleon-nucleon bremsstrahlung, and q_{plasmon}^- is the cooling rate by plasmon decays (Kohri & Mineshige 2002; Di Matteo, Perna & Narayan 2002). In the following expressions, we omit the Fermi-blocking effect by the background neutrinos in the final state. We discuss this point later.

The electron-positron capture rate by nucleons is represented by the sum of two terms:

$$q_{Ne}^- = q_{p+e^- \rightarrow n+\nu_e}^- + q_{n+e^+ \rightarrow p+\bar{\nu}_e}^-, \quad (47)$$

with

$$q_{p+e^- \rightarrow n+\nu_e}^- = \frac{G_F^2}{2\pi^3 \hbar^3 c^2} (1 + 3g_A) n_p \int_Q^\infty dE_e E_e \sqrt{E_e^2 - m_e^2 c^4} (E_e - Q)^3 \frac{1}{e^{(E_e - \mu_e)/k_B T} + 1}, \quad (48)$$

$$q_{n+e^+ \rightarrow p+\bar{\nu}_e}^- = \frac{G_F^2}{2\pi^3 \hbar^3 c^2} (1 + 3g_A) n_n \int_{m_e c^2}^\infty dE_e E_e \sqrt{E_e^2 - m_e^2 c^4} (E_e + Q)^3 \frac{1}{e^{(E_e + \mu_e)/k_B T} + 1}, \quad (49)$$

where $G_F = 2.302 \times 10^{-22} \text{cm MeV}^{-1}$, and the axial vector coupling constant $g_A \simeq 1.4$, determined by the experimental value of the neutron lifetime (see § 2.2.2). We plot the two cooling terms in the T – η_e plane in Fig. 2 (c) and Fig. 2 (d), respectively. The rates are normalized by the number density of the nucleon (i.e., proton or neutron) in the initial state.

The electron-positron pair annihilation rate into neutrinos is the sum of the contributions from the three lepton generations:

$$q_{e^+e^-}^- = \sum_{i=e,\mu,\tau} q_{e^+e^- \rightarrow \nu_i \bar{\nu}_i}^-, \quad (50)$$

⁴As per the approximations in Di Matteo, Perna & Narayan (2002), for simplicity, the difference of the optical depths between ν_e and $\bar{\nu}_e$ is ignored. This simplification does not change our conclusion so much.

with

$$q_{e^+e^- \rightarrow \nu_e \bar{\nu}_e}^- = 3.4 \times 10^{33} \text{ erg cm}^{-3} \text{ s}^{-1} \left(\frac{T}{10^{11} \text{ K}} \right)^9, \quad (51)$$

$$q_{e^+e^- \rightarrow \nu_\mu \bar{\nu}_\mu}^- = q_{e^+e^- \rightarrow \nu_\tau \bar{\nu}_\tau}^- = 0.7 \times 10^{33} \text{ erg cm}^{-3} \text{ s}^{-1} \left(\frac{T}{10^{11} \text{ K}} \right)^9. \quad (52)$$

These expressions are valid in the nondegenerate limit $\eta_e \ll 1$. If the electrons are degenerate, the electron-positron pair annihilation rate becomes quite small, compared with the other neutrino cooling processes. We therefore neglect the pair annihilation term whenever $\eta_e \ll 1$.

The nucleon-nucleon bremsstrahlung rate through the process $n + n \rightarrow n + n + \nu + \bar{\nu}$ is represented by

$$q_{\text{brems}}^- = 1.5 \times 10^{33} \text{ erg cm}^{-3} \text{ s}^{-1} \left(\frac{T}{10^{11} \text{ K}} \right)^{5.5} \left(\frac{\rho}{10^{13} \text{ g cm}^{-3}} \right)^2, \quad (53)$$

where we consider only the case when the nucleons are not degenerate (Hannestad & Raffelt 1998; Burrows et al. 2000).

Plasmon decay into neutrinos is most effective at high density and high electron degeneracy (Schinder et al. 1987). The plasmons $\tilde{\gamma}$ are photons interacting with electrons. The decay rate into ν_e and $\bar{\nu}_e$ of transverse plasmons is given by

$$q_{\text{plasmon}}^- = 1.5 \times 10^{32} \text{ erg cm}^{-3} \text{ s}^{-1} \left(\frac{T}{10^{11} \text{ K}} \right)^9 \gamma_p^6 e^{-\gamma_p} (1 + \gamma_p) \left(2 + \frac{\gamma_p^2}{1 + \gamma_p} \right), \quad (54)$$

where $\gamma_p = 5.565 \times 10^{-2} \sqrt{(\pi^2 + 3\eta_e^2)/3}$ (Ruffert, Janka & Schäfer 1996). Note that the process $\tilde{\gamma} \rightarrow \nu_e + \bar{\nu}_e$ is more effective by a factor of ~ 163 , compared with that of the other flavors, $\rightarrow \nu_\mu \bar{\nu}_\mu$ and $\nu_\tau \bar{\nu}_\tau$.

Having discussed the various cooling terms, we now introduce various “optical depths” of the different neutrinos. The absorption optical depths of the three neutrino species $\nu_i = \nu_e, \nu_\mu$, and ν_τ are defined by

$$\tau_{a, \nu_e} = \frac{\left(q_{p+e^- \rightarrow n + \nu_e}^- + q_{e^+e^- \rightarrow \nu_e \bar{\nu}_e}^- + q_{\text{brems}}^- + q_{\text{plasmon}}^- \right) H}{(7/2) \sigma T^4}, \quad (55)$$

$$\tau_{a, \nu_\mu} = \tau_{a, \nu_\tau} = \frac{\left(q_{e^+e^- \rightarrow \nu_\mu \bar{\nu}_\mu}^- + q_{\text{brems}}^- \right) H}{(7/2) \sigma T^4}. \quad (56)$$

According to Tubbs & Schramm (1975), Shapiro & Teukolsky (1983), and Di Matteo, Perna & Narayan (2002), the scattering optical depth of neutrinos through elastic scattering off background nucleons, $\nu_i + \{n \text{ or } p\} \rightarrow \nu_i + \{n \text{ or } p\}$, is the same for all three species and is given by

$$\tau_{s,\nu_i} = 7.7 \times 10^{-7} (C_{s,p} Y_p + C_{s,n} Y_n) T_{11}^2 \rho_{10} H. \quad (57)$$

Here $C_{s,p} = [4(C_V - 1)^2 + 5\alpha_a^2]/24$ and $C_{s,n} = (1 + 5\alpha_a^2)/24$, with the vector coupling $C_V = 1/2 + 2\sin^2 \theta_W$, and $\alpha_a \approx 1.25$. The Weinberg angle is $\sin^2 \theta_W = 0.23$ (Eidelman et al. 2004).

Using the above optical depths of neutrinos, we write the total neutrino cooling rate as

$$\begin{aligned} Q_\nu^- &= \sum_{i=e,\mu,\tau} \frac{(7/8)\sigma T^4}{(3/4) [\tau_{\nu_i}/2 + 1/\sqrt{3} + 1/(3\tau_{a,\nu_i})]} \\ &= 6.62 \times 10^{39} T_{11}^4 \text{ erg cm}^{-3} \text{ s}^{-1} \sum_{i=e,\mu,\tau} \frac{1}{[\tau_{\nu_i}/2 + 1/\sqrt{3} + 1/(3\tau_{a,\nu_i})]}, \end{aligned} \quad (58)$$

where the total optical depth of the neutrino is $\tau_{\nu_i} = \tau_{a,\nu_i} + \tau_{s,\nu_i}$. The above expression is based on the work of Popham & Narayan (1995) and is designed to operate in both the optically very thin and optically very thick limits. It represents a bridging formula between these two limits and provides a reasonable estimate of the cooling rate in the difficult but important intermediate regime where τ is of order a few.

Note that the optical depths discussed above provide some information on whether or not neutrinos are thermalized in the electromagnetic thermal bath (provided the timescale for collisions is shorter than the dynamical timescale⁵). Because we do not explicitly solve the Boltzmann equation for the time evolution of the energy distribution of neutrinos and the energy transfer, we conservatively regard the above neutrino optical depths as an indicator of the degree of thermalization of neutrinos. That is, when all the τ 's are larger than 2/3, we assume the neutrinos to be thermalized.

For the other scattering processes except neutrino-nucleon scattering ($\nu_i + \{n \text{ or } p\} \rightarrow \nu_i + \{n \text{ or } p\}$), there also exists the possibility of elastic scattering off background electrons (positrons), $\nu + e \rightarrow \nu + e$. The energy dependence (or temperature dependence) of this reaction rate is similar to that of neutrino-nucleon collisions. However, its contribution to

⁵We have checked the competition among various timescales in Appendix A. We find that the timescale for neutrino collisions is much shorter than the dynamical timescale in the parameter space where the optical depths are larger than 2/3.

the optical depth is subdominant or comparable at most in the electron-degeneracy regime. Therefore, for simplicity we have omitted it in the calculation of the neutrino optical depth.⁶

Finally we note that, when we calculate the neutrino-cooling rates, we omit the Fermi-blocking effect by the background neutrinos. We believe that this approximation is reasonable. When the accreting gas is transparent to neutrinos ($\tau's \ll 1$), the approximation is obviously good since the produced neutrinos are not thermalized, and so we can omit the neutrino-neutrino scattering. On the other hand, when the gas becomes opaque to neutrinos, we strongly suppress the neutrino-cooling rates by introducing the optical depths τ in Eq. (58). Since the suppression effect due to optical depth is typically much stronger than the suppression due to Fermi-blocking for $\tau's \gg 1$, we believe it is reasonable to ignore the latter.

2.4. Comparison to previous work

Several aspects of our model are similar to previous treatments of the problem (Narayan, Piran & Kumar 2001; Kohri & Mineshige 2002; Di Matteo, Perna & Narayan 2002), though our work goes significantly further in handling the details. The original model of Narayan et al. (2001) made use of a simple neutrino-cooling rate, which was then improved by Kohri & Mineshige (2002) who pointed out that it is important to include the effect of electron degeneracy which suppresses the neutrino-cooling rate at high density and high temperature. Di Matteo, Perna & Narayan (2002) pointed out that the accreting gas could be optically thick to neutrino emission, so that a neutrinosphere could form at high temperatures and thereby suppress neutrino emission. The accretion flow then becomes advection-dominated⁷.

Our model includes the effects of electron degeneracy and neutrino optical depth in calculating physical quantities such as neutrino-cooling rates, matter density, temperature, pressure, etc. In this connection, we have taken greater care to calculate the neutron to proton ratio n/p as accurately as possible since this ratio has a large effect on the neutrino-cooling rates and the electron chemical potential. Although the importance of n/p was also

⁶For energy transfer of neutrinos, however, the scattering off background electrons might be more important than scattering off nucleons. Thus, if we were to explicitly solve the Boltzmann equation for the energy transfer of neutrinos, we would have to include the elastic collisions between neutrinos and electrons.

⁷Recently, we noticed that Yokosawa, Uematsu & Abe (2004) studied models of the neutrino-cooled disk without explicitly adopting the advective cooling term. Their results are different from those in Narayan, Piran & Kumar (2001), Kohri & Mineshige (2002), and Di Matteo, Perna & Narayan (2002), as they have admitted.

stressed by Kohri and Mineshige (2002), their approach was a great deal simpler. Here we have considered the competition among various timescales in determining the equilibrium between neutrons and protons, and we have also checked under what conditions neutrinos are thermalized.

Furthermore, we have calculated various quantities such as the neutrino cooling rates, the interconversion rates between neutrons and protons, the electron pressure, and the electron number densities by numerically integrating the distribution function of electrons over momentum. We are thus able to calculate these quantities even in the delicate regime where the electron degeneracy is moderate. This is a significant improvement over previous works which were restricted to calculating quantities only in the two opposite limits of extremely degenerate electrons and fully non-degenerate electrons.

2.5. Results for the disk structure

Using the model described in the previous subsections, we can calculate all the properties of a neutrino-cooled accretion disk for any large mass accretion rate. Given the mass m of the accreting compact core, the mass accretion rate \dot{m} , and the radius r (all in dimensionless units, see Eqs. (1), (2) and (3)), and using the various subsidiary relations written down earlier, we numerically solve the energy balance condition (heating rate = cooling rate),

$$Q^+ = Q^-. \quad (59)$$

The solution gives the various quantities of interest such as the mass density ρ , the temperature T , the surface density Σ , etc.

Fig. 3 shows contours of the advection parameter $f_{\text{adv}} \equiv (H/R)^2$ in the r – \dot{m} plane for $m = 1.4$ (corresponding to a proto-neutron star at the center) and $\alpha = 0.1$. Note the qualitative similarity of this plot to the middle panel of Fig. 3 in Di Matteo, Perna & Narayan (2001). However, the present calculations are more accurate and also correspond to a different mass (Di Matteo et al. considered $m = 3$). In this plot, regions with f_{adv} close to unity are highly advection-dominated, whereas regions with $f_{\text{adv}} < 0.5$ are cooling-dominated and have significant neutrino emission.

Figs. 4 (a) and (b) show contours of density and temperature, respectively, in the r – \dot{m} plane. Both quantities increase toward the upper left region of the diagram. The degeneracy parameter η_e is shown in Fig. 4 (c). There is a tendency for η_e to increase toward the upper right region.

In Fig. 4 (d), we show which of the various terms in Q^- dominates in which regions of

the plane. As already mentioned, radiative cooling is never important at these ultra-high mass accretion rates. Neutrino cooling, on the other hand, does become important over an extended region of the plane near the middle of the plot. The most important emission process here is electron-positron capture. Not surprisingly, the region where neutrino cooling dominates overlaps with the region where f_{adv} is small in Fig. 3, i.e., where advection is not important.

Figures 3 and 4 (d) show that advection is important over much of the rest of the plane. The reason is easy to understand. Contours of τ_{a,ν_e} and τ_{s,ν_e} are shown in Fig. 5 (a) and Fig. 5 (b), with the thick lines corresponding to $\tau = 2/3$. From these plots, we see that the disk becomes “optically thick” to neutrino emission, and a neutrinosphere is formed, in the upper left region of the plane. This suppresses neutrino cooling in this region of parameter space, causing the flow to become advection-dominated. In the bottom right region, the optical depth is very small, but the emission processes themselves are weak and so once again the flow is advection-dominated.

In the right-most region of Fig. 4 (d), cooling due to photo-dissociation dominates. This is indicated in Fig. 6 (a), which shows contours of the nucleon fraction X_{nuc} in the $r-\dot{m}$ plane. For $r \lesssim 150$, we find that approximately $X_{\text{nuc}} \sim 1$. Therefore, for these radii which are the parameter space of interest to us, most of the nuclei have been completely dissociated into free nucleons in the thermal bath. We may omit (for simplicity) the cooling due to photodissociation of heavy nuclei in Eq. (39) in this region of the plane. At larger radii, photodissociation is important and dominates the cooling.

In Fig. 6 (b) we show the neutron to proton ratio. We see that n/p is larger than unity over much of the parameter space. This is because electrons are highly degenerate and have positive values of η_e . We then expect an excess of neutrons. This neutron rich gas with a short dynamical timescale ($\ll 1$ s) might lead to r -process nucleosynthesis (Hoffman, Woosley & Qian 1997), as we discuss in § 3.5. In Fig. 6 (c) the dominant component of the pressure (see § 2.2 for a definition of the various components) is shown in the $r-\dot{m}$ plane. We see that gas pressure dominates in the region where the neutrino cooling is effective. Finally, in Fig. 6 (d) we plot contours of the net number density of electrons n_e .

3. Outflow Energy From the Disk

In this section we present several different estimates of the mechanical energy in the wind flowing out from a neutrino-dominated disk during core-collapse of a massive star. We begin in § 3.1 with a simple discussion of the relevant physics and follow this up in succeeding

subsections with more detailed calculations.

3.1. Qualitative Estimate of Outflow Energy

Before going into detailed calculations, we first present a simple qualitative estimate of the energy that might be carried out by the disk outflow. A vigorous outflow is expected whenever the accretion flow is advection-dominated (Narayan & Yi 1994, 1995a). Although the calculations in § 2.5 and the results shown in Fig. 3 indicate that advection does not dominate for all parameters of interest, let us for simplicity assume here that the disk is always advection-dominated. Since an outflow carries away mass, the accretion rate in the disk will decrease with decreasing radius. For simplicity, let us assume that the accretion rate varies as a power-law in radius,

$$\dot{M}(r) = \dot{M}_0 \left(\frac{r}{r_0} \right)^s, \quad (60)$$

with a constant index s . Here r_0 is the radius of the outer edge of the disk and \dot{M}_0 is the mass accretion rate at that radius. The differential rate of outflow of mass in the wind is then given by

$$d\dot{M} = \frac{s\dot{M}_0}{r_0^s} \frac{dr}{r^{1-s}}. \quad (61)$$

The terminal velocity of the outflowing gas is likely to be of the order of the escape velocity from the point of origin in the disk, $v_{\text{esc}} = \sqrt{GM/R} = c/\sqrt{2r}$. Let us therefore write the specific energy (at infinity) of the wind as $(1/2)\xi v_{\text{esc}}^2$, where the fudge factor $\xi \sim 0.1 - 1$ absorbs our ignorance of the details of the outflow. The differential rate of outflow of energy in the wind is then

$$d\dot{E}_w = \xi \frac{GM}{R} d\dot{M} = \frac{s\xi\dot{M}_0 c^2}{2} \frac{dr}{r_0^s r^{2-s}}. \quad (62)$$

Let us assume that the scaling of \dot{M} given in Eq. (60) extends from $r = r_0$ on the outside down to an innermost radius $r = r_{\text{in}}$. Integrating over r , we then estimate the total rate of outflow of energy in the wind to be

$$\dot{E}_w = \begin{cases} \frac{s}{2(1-s)} \frac{\xi\dot{M}_0 c^2}{r_0^s} \left(\frac{1}{r_{\text{in}}^{1-s}} - \frac{1}{r_0^{1-s}} \right), & \text{for } s < 1, \\ \frac{s\xi\dot{M}_0 c^2}{2} \frac{1}{r_0} \ln \left(\frac{r_0}{r_{\text{in}}} \right), & \text{for } s = 1. \end{cases} \quad (63)$$

If the compact core at the center is a non-spinning black hole, then we expect $r_{\text{in}} = 3$ (innermost stable circular orbit in a Schwarzschild space-time), and if it is a spinning hole then r_{in} would be even smaller. For a proto-neutron star, however, the inner edge of the accretion flow will be significantly larger. If the mass of the core is $1.4M_{\odot}$ and its radius is about 30 km (e.g., Lattimer & Prakash 2004), then we have $r_{\text{in}} \sim 7$, which is the value we assume below.

Consider first the second line of equation (63) which corresponds to the limit $s = 1$. We see that the outflow energy decreases with increasing outer radius. This is because $s = 1$ corresponds to a very heavy mass outflow rate; in fact, it is the maximum likely value of s (see Blandford & Begelman 1999). Even though the specific energy of the outflowing matter increases at smaller radius, the amount of mass available at small radii is greatly reduced. Therefore, the overall scale of the energy outflow is determined primarily by the outer radius, and we get equal contributions to the outflow energy from equal logarithmic intervals of radius, hence the logarithmic factor. Figure 7 shows a plot of \dot{E}_w versus r_0 . We see that for $s = 1$ the maximum energy outflow rate is obtained for $r_0 \sim 15$. At smaller radii, even though the overall energy scale is larger, the value of the logarithm becomes small and this causes a reduction in the outflow energy.

In the opposite limit, when s is close to 0, we see from the first line of equation (63) that the energy outflow rate is proportional to $s\dot{M}_0/r_{\text{in}}$. Here, the rate is almost independent of r_0 because the energy outflow is dominated by small radii. In fact, what matters now is how much mass is expelled in the outflow near r_{in} , which by equation (61) is proportional to s . When s is exactly equal to 0, there is obviously no outflow at all and hence the outflow energy vanishes. Figure 7 shows the behavior of the outflow energy for intermediate values of s between 0 and 1. The overall pattern is easy to understand in terms of the two limiting cases discussed above.

Quantitatively, Fig. 7 shows that $\dot{E}_w/\xi\dot{M}_0c^2$ is in the range 0.01 to 0.05 for reasonable choices of r_0 and s . In other words, for every solar mass supplied to the disk at the outer edge r_0 , an amount of energy $\sim (2 - 10) \times 10^{52}\xi$ erg is expected to flow out of the disk in the wind. Even if we conservatively take ξ to be 0.1, this is still a substantial amount of energy. We have, however, assumed in the present discussion that the disk is highly advection-dominated throughout and that it ejects a strong outflow for all combinations of \dot{M} and R . In reality, the accretion flow in an NDAF is only partially advection-dominated and the degree of advection varies as a function of mass accretion rate and radius. In the following subsections we obtain better estimates of the energy in the outflow.

3.2. More Quantitative Results

To allow for the effect of variable advection, let us generalize equation (61) to

$$\frac{d \ln \dot{M}}{d \ln R} = s(R) \geq 0, \quad (64)$$

i.e.,

$$\frac{d \dot{M}}{d R} = s(R) \frac{\dot{M}}{R}, \quad (65)$$

where the index s is now no longer considered to be a constant but is allowed to vary with radius. As already mentioned, we expect outflows to be important when the accreting gas is advection-dominated and to be negligible when the gas is able to cool readily. Based on this insight, Yuan, Cui & Narayan (2004) came up with the following simple prescription for the outflow index:

$$s(R) = s_0 f(R) = s_0 f_{\text{adv}}, \quad (66)$$

where s_0 is a constant, and $f_{\text{adv}} = Q_{\text{adv}}^-/Q^+ \approx (H/R)^2$ measures the degree of advection in the flow (see eq. (46)). Although Yuan et al. (2004) proposed this model for advection-dominated flows in X-ray binaries, the arguments behind it are general and should apply also to an NDAF.

The differential outflow energy flux produced between radii r and $r + dr$ is

$$d\dot{E}_w = \frac{1}{2} \xi v_{\text{esc}}^2 d\dot{M} = s(r) \frac{\dot{M}}{r} \frac{\xi c^2}{4r} dr, \quad (67)$$

where ξ is the same fudge factor introduced in § 3.1. Integrating from $r = r_0$ down to $r = r_{\text{in}}$ we obtain the total rate of energy outflow from the disk \dot{E}_w . In Fig. 8, we show contours of $\dot{E}_w/(\xi \dot{M}_0 c^2)$ in the r_0 – \dot{m}_0 plane (where $\dot{m}_0 = \dot{M}_0/M_\odot \text{s}^{-1}$) for different choices of the outflow index: $s_0 = 0.3, 0.5, 0.7$, and 0.9 . For a wide range of r_0 and \dot{M}_0 , we see that roughly $(0.1 - 1)\xi$ % of the rest mass energy of the accreting gas comes out in the form of kinetic energy in the wind. The energy estimate is somewhat lower than the one given in § 3.1, mainly because the disk is only moderately advection-dominated over wide ranges of the parameters. Nevertheless, if $\dot{M}_0 = 1 M_\odot \text{s}^{-1}$ ($0.1 M_\odot \text{s}^{-1}$), then \dot{E}_w is $(10^{51} - 10^{52})\xi \text{ erg s}^{-1}$ [$(10^{50} - 10^{51})\xi \text{ erg s}^{-1}$]. Thus, even for fairly small values of \dot{M}_0 , we find that the outflow energy is still quite significant.

What value of s_0 should we use for the outflow? The limit $s_0 = 0$ corresponds to the original ADAF (Narayan & Yi 1994; 1995a) in which there is no outflow, while $s_0 = 1$

corresponds to the extreme limit of a convection-dominated accretion flow (CDAF; Narayan, Igumenshchev & Abramowicz 2000; Quataert & Gruzinov 2000) which deviates maximally from the ADAF. Values of s_0 in between correspond to generalized wind models (Blandford & Begelman 1999). Numerical hydro and MHD simulations give s_0 anywhere in the range from about 0.7 to 1 (Igumenshchev et al. 2000; 2003; Pen et al., 2003). On the other hand, a model for the accreting supermassive black hole Sgr A* at the Galactic Center gives $s_0 \sim 0.3$ (Yuan et al. 2003). It is probably best to keep an open mind on the value of s_0 , though larger values should perhaps be favored.

The results shown in Figure 8 correspond to a viscosity parameter $\alpha = 0.1$. While this is a reasonable value, it is of interest to investigate how the results change for other values. Figure 9 shows the effect of changing α to 0.01. We see that the contours in the lower half of the various panels are shifted downward by about two orders of magnitude in \dot{M}_0 . (Note that the vertical axis extends over a larger range in Figure 9.) The effect is exactly the same as for ADAFs with *radiative cooling*. As explained in Narayan & Yi (1995b; see also Narayan, Mahadevan & Quataert 1998), at low Eddington ratios, the transition from a radiatively efficient accretion flow to an advection-dominated accretion flow (ADAF) occurs at a critical mass accretion rate $\dot{M}_{\text{crit}} \propto \alpha^2$. This scaling arises because the cooling rate per unit mass of the accreting gas is proportional to ρ , which is proportional to $\dot{M}\alpha^{-1}$, so that the cooling time of the gas varies as $t_{\text{cool}} \propto \alpha/\dot{M}$. On the other hand, the accretion time varies as $t_{\text{acc}} \propto \alpha^{-1}$. Thus, the condition $t_{\text{cool}} = t_{\text{acc}}$, which represents the transition from a radiatively efficient flow to an ADAF, leads to $\dot{M}_{\text{crit}} \propto \alpha^2$. In an NDAF, the cooling is via neutrinos. However, the cooling rate per unit mass is still proportional to the density and so the same scaling continues to hold.

3.3. Application to Supernovae — Prompt Explosion

In this and the following subsection, we consider two distinct (idealized) scenarios in which the outflow from an NDAF might cause a supernova explosion. Here we suppose that the collapsing stellar core has a fairly large specific angular momentum so that immediately after the initial homologous collapse, we have a proto-neutron star core plus some additional material in a surrounding accretion disk. The disk forms nearly on a dynamical time, which is much shorter than the viscous time of the orbiting gas. Thus, we have a fully formed disk at a particular instant $t = 0$ and we follow the depletion of the mass in the disk as a result of viscous accretion and outflow. The question we are interested in is how much energy flows out in the wind and whether this energy is enough to cause a successful prompt supernova explosion.

Let us assume that the disk initially consists of a mass

$$M_d(0) \equiv M_d(t = 0), \quad (68)$$

with the bulk of the mass lying at some characteristic radius $R_0 = r_0 R_S$, which we will think of as the “outer radius” of the disk. For clarity, in this subsection we explicitly write the argument of functions such as t and R . From equations (32) and (33), we see that the viscous timescale at radius R is given by

$$t_{\text{visc}}(t, R) = \frac{R}{v_R(t, R)} \sim \frac{2}{3\alpha} \frac{R^2 \Omega_K(R)}{[c_s(t, R)]^2}. \quad (69)$$

The mass accretion rate at the outer radius R_0 is then approximately given by

$$\dot{M}_0(t) \equiv \dot{M}(t, R = R_0) = -dM_d(t)/dt \sim M_d(t)/t_{\text{visc}}(t, R_0), \quad (70)$$

where $\dot{M}(t, R)$ refers to the mass accretion rate at a given time t and at a radius R . The above equation gives both the mass accretion rate at the outer edge at a given time and the rate at which the total disk mass decreases. In addition, at a given time, $\dot{M}(t, R)$ decreases with decreasing R according to equations (65) and (66) written down earlier. Finally, we need a prescription for the evolution of the characteristic outer radius of the disk. For simplicity, we assume that the radius does not change with time. We then have a complete prescription for the temporal and radial variation of the accretion rate $\dot{M}(t, R)$. The time evolution of the disk mass $M_d(t)$ is obtained by solving Eq. (70),

$$M_d(t) = M_d(0) \exp \left[- \int_0^t d\tau \frac{1}{t_{\text{visc}}(\tau, R_0)} \right]. \quad (71)$$

Equivalently, the time evolution of the outer mass accretion rate $\dot{M}_0(t) = \dot{M}(t, R_0)$ is given by

$$\dot{M}_0(t) = \dot{M}_0(0) \frac{t_{\text{visc}}(0, R_0)}{t_{\text{visc}}(t, R_0)} \exp \left[- \int_0^t d\tau \frac{1}{t_{\text{visc}}(\tau, R_0)} \right] \quad (72)$$

With these formulae, for given initial disk mass $M_d(0)$, outer radius $r_0 = R_0/R_S$ and outflow index s_0 , we can calculate the complete evolution of the disk and estimate the total energy, integrated over radius and time, carried out by the outflow. Figure 10 shows some numerical results.

In Fig. 10(a) we plot contours of the total outflow energy E_w/ξ in the $r_0 - M_d(0)$ plane for $s_0 = 0.5$. For any value of $\xi \neq 1$, the outflow energy is obtained by taking the value given in the plot and multiplying by ξ . Note that E_w/ξ exceeds 10^{50} erg over a wide region

of parameter space, in particular for $M_d(0) \gtrsim 10^{-2} M_\odot$ and $r_0 \sim 10 - 100$. In Fig. 10(b), we show E_w/ξ as a function of s_0 for selected values of the disk mass: $M_d(0)/M_\odot = 10^{-2}$, 5×10^{-2} , 0.1, 0.5, and 1. Here we have set $r_0 = 20$. Note again that the outflow energy is fairly substantial, especially if the disk mass is $0.1 M_\odot$ or more. These results show that the outflow can help to produce a prompt supernova explosion provided there is enough mass in the initial accretion disk.

3.4. Application to Supernovae — Delayed Explosion

In this subsection we consider a different scenario. Let us suppose that the initial collapse does not lead to a prompt explosion, either because there is not enough angular momentum in the core to form an accretion disk or because there is insufficient mass in the disk. The system will transition to a fairly long-lived state (several seconds) in which material will flow in through the stalled shock towards the central core. As time progresses, the infalling material will originate from larger and larger radii in the pre-collapse star and it is quite likely that the angular momentum of the gas will be sufficient to produce a centrifugally-supported fallback disk. For a core of mass $1.4 M_\odot$ and a radius of 30 km, the critical specific angular momentum needed to form a disk is $\ell_{\text{crit}} \sim 2.5 \times 10^{16} \text{ cm}^2 \text{ s}^{-1}$. This level of angular momentum is not unusual for a collapsing star (e.g., Mineshige et al. 1997; Heger, Langer & Woosley 2000).

From a computational point of view, the present scenario differs from the one described in the previous subsection primarily in the relative magnitude of time scales. Previously, we assumed that the fallback time over which matter is added to the disk t_{fallback} is much shorter than the viscous timescale t_{visc} over which a given parcel of gas flows through the disk, i.e., $t_{\text{fallback}} \ll t_{\text{visc}}$. Thus, the time evolution of the disk is primarily determined by t_{visc} . In contrast, here we assume that the viscous timescale is much shorter than the fallback time: $t_{\text{visc}} \ll t_{\text{fallback}}$. Thus, the time evolution is determined by t_{fallback} .

Assuming that a disk forms during the fallback stage, it is clear that a considerable amount of outflow energy will be generated in the present scenario. This is because a failed supernova has few to several solar masses of fallback material. Even if only a fraction of this mass goes into the disk, the outflow energy would still be considerable. To get some numerical estimates, let us assume that the fallback material rains down at some “outer” radius R_0 at an initial rate $\dot{M}_0(0)$. Let us also assume that the mass inflow rate declines exponentially with time with a characteristic decay time \bar{t} ,

$$\dot{M}_0(t) = \dot{M}_0(0) \exp(-t/\bar{t}), \quad \text{for } t \geq 0, \quad (73)$$

Note that the subscript “0” means the value at $R = R_0$. The variation of \dot{M} with R is as in equations (65) and (66). In this simple model, the total amount of mass flowing into the disk at R_0 is $\bar{t}\dot{M}_0(0)$.

In Fig. 11 (a), we plot contours of the time- and radius-integrated total outflow energy as a function of the initial accretion rate $\dot{M}_0(0)$ and the outer radius r_0 . For simplicity, we have assumed that r_0 is independent of time (see below for a more realistic model), and we have adopted $\bar{t} = 1$ s, $s_0 = 0.5$, $M = 1.4M_\odot$, $\alpha = 0.1$, and $r_{\text{in}} = 7$. The numerical values shown are for $\xi = 1$ and should be multiplied by ξ for other values of this parameter. Because we have taken $\bar{t} = 1$ s, the vertical range in the plot corresponds to a total fallback mass ranging from $0.1M_\odot$ at the bottom to $1M_\odot$ at the top. Even for this fairly modest mass budget, we see that the outflow energy is quite significant.

Next, we attempt a more realistic calculation using numerical simulations of core-collapse supernovae as a guide. Livne (2004) has presented results corresponding to the collapse of a $11M_\odot$ progenitor star. At a particular time, the shock is at $R = 240$ km ($r_0 = 57$ for a compact core of mass $M = 1.4 M_\odot$), and the fluid velocity, density, pressure and temperature on the two sides of the shock are as in Table 1. Let us call the upstream (downstream) region of the shock as “region I” (“region II”). Hereafter, the subscript I (II) refers to physical quantities in the particular region.

Using the Rankine-Hugoniot relation for the product of the velocity and the matter density, which is defined in the rest frame of the shock front, we find that

$$v_{\text{rest}} \rho_{\text{rest}} = (v_{\text{I}} - v_{\text{sh}})\rho_{\text{I}} = (v_{\text{II}} - v_{\text{sh}})\rho_{\text{II}}, \quad (74)$$

where v_{sh} is the velocity of the shock front in the rest frame of the central star. Substituting the values in Table 1 into Eq. (74), we see that $v_{\text{sh}} = 2.7 \times 10^8 \text{ cm s}^{-1}$. That is, the shock front is not completely stalled but is gradually moving outward. The mass accretion rate can be roughly obtained by $\dot{M}_0 \sim 4\pi r_0^2 \rho_{\text{rest}} v_{\text{rest}} \sim 0.6M_\odot \text{ s}^{-1}$. Using the analysis presented

Table 1. Physical quantities around the shock front at $R = 240$ km in the numerical simulations of core-collapsed supernova. In this case, the progenitor star has an eleven solar mass (Livne 2004).

	v (cm s $^{-1}$)	ρ (g cm $^{-3}$)	p (erg cm $^{-3}$)	T (K)
upstream (I-region)	-3.0×10^9	5.0×10^7	2.0×10^{25}	6.4×10^9
downstream (II-region)	-2.0×10^8	3.5×10^8	8.0×10^{26}	1.3×10^{10}

earlier in this subsection, we can estimate the total time-integrated outflow energy E_w if the shock front is stationary. For instance, for $(r_0, \dot{M}_0) = (57, 0.6M_\odot\text{s}^{-1})$, Fig. 11 (a) gives $E_w \sim 3 \times 10^{51}$ erg, if we take $\bar{t} = 1$ s.

However, since we have estimated the outward speed of the shock and know that it is not zero, let us also calculate the results for this particular case. Although we do not know the exact behavior of the shock front as a function of time, numerical simulations of core-collapse supernovae generally show that the shock front stalls after a short time $\lesssim 1$ s. Therefore, for simplicity, we assume that the velocity of the shock front evolves as

$$v_{\text{sh}}(t) = v_{\text{sh}}(0) \exp(-t/\bar{t}), \quad \text{for } t \geq 0, \quad (75)$$

where we use the same \bar{t} as in Eq. (73). Thus, the position of the shock front evolves as

$$\begin{aligned} r_0(t) &= r_0(0) + \int_0^t v_{\text{sh}}(t) dt \\ &= r_0(0) + v_{\text{sh}}(0) \bar{t} [1 - \exp(-t/\bar{t})], \end{aligned} \quad (76)$$

where $r_0(0) = 57$ and $v_{\text{sh}}(0) = 2.7 \times 10^8 \text{cm s}^{-1}$.

In Fig. 11 (b), we plot the time-integrated total outflow energy E_w as a function of s_0 for three choices of \bar{t} : 0.5, 1, and 2 s. From the figure, we see that the outflow energy is $E_w \sim 10^{51-52} \xi$ erg over a wide range of values of s_0 .⁸ The total mass supplied to the fallback disk is $0.3M_\odot$, $0.6M_\odot$, $1.2M_\odot$, respectively, for the three choices of \bar{t} considered in this calculation. This is quite conservative because we expect much more mass to be available in a failed supernova. Even so, and even if we make the conservative assumption that $\xi \sim 0.1$, we see that quite a lot of energy is expected in the outflow.

One additional point is that, in the delayed supernova scenario, the continued longtime accretion will tend to increase the mass of the remnant neutron star. This may help resolve a problem in some classes of simulations (Herant et al. 1994; Burrows et al. 1995; Scheck et al. 2004), viz., that the mass of the neutron star predicted in these simulations is less than $1.4 M_\odot$.

⁸Because we terminated the numerical calculation for $R > 10^8 \text{cm}$, these numerical values are conservative lower bounds on the outflow energies. However, we checked that, even if we include the contribution from $R > 10^8 \text{cm}$, it does not change the results significantly.

3.5. Nuclear Reactions in the Outflow

The outflowing material in the disk outflow begins as dissociated nucleons, but as it flows out and cools, it will undergo nuclear reactions of various kinds (MacFadyen 2003). We briefly touch on some interesting phenomena that may be expected as a result.

As discussed in §2.5 and shown in Fig. 6 (a), the photodissociation of nuclei in the accretion flow acts as an effective cooling term. Correspondingly, the recombination of nucleons into nuclei in the outflow is exothermic and increases the energy available in the outflow. The energy release is about 8 MeV per nucleon (MacFadyen 2003), which is substantial. This energy was not included in the energy estimates obtained in the previous subsections. Figure 12 shows how those results are modified when the recombination energy is included. In the new calculations, the outflowing gas at each radius is assumed to start off with X_{nuc} equal to the value given in equation (40), and the energy release from this material is calculated assuming that each free nucleon releases 8 MeV through recombination. The particular case shown is for $\xi = 0.1$. A comparison with Figure 8 shows that the recombination energy is quite substantial. Without including this energy, for $\xi = 0.1$ the maximum efficiency of the outflow for the optimum choice of r_0 and \dot{m}_0 is only $\dot{E}/\dot{M}_0 c^2 \sim 10^{-3}$, whereas with the recombination energy included the efficiency can become as high as 8×10^{-3} .

Another interesting possibility is suggested by Fig. 6 (b), where we see that the neutron to proton ratio in the disk is quite high over large regions of parameter space. Such a neutron rich region with a short dynamical timescale ($\ll 1$ s) is likely to be the site of r -process nucleosynthesis (Hoffman, Woosley & Qian 1997).⁹ The interesting thing in our model is that the neutron rich material flows out as part of the advection-induced wind. During the outflow, r -process elements could be generated and these will be ejected by the supernova explosion. This possibility has been explored by various authors within the context of gamma-ray bursts and the collapsar model (Pruet et al. 2003, 2004a,b; Fujimoto et al. 2004; Surman & McLaughlin 2004, 2005). Our proposal is that similar considerations should apply also in the context of regular supernovae.

It should be noted that there is at present no accepted model for successful r -process nucleosynthesis (see recent papers by Qian & Wasserburg 2002 and Qian 2005). From the viewpoint of event rates, the core-collapse supernova is a more likely site for r -process nucleosynthesis than the binary neutron star merger (Eichler et al. 1989; Freiburghaus et al. 1999). This is because even in metal poor stars with $\text{Fe}/\text{Fe}_\odot = 10^{-4} - 10^{-3}$, typical r -process

⁹For the neutron capture reaction to be more rapid than β -decay, we need a large neutron flux ($\gtrsim 10^{31} \text{cm}^{-2} \text{s}^{-1}$). Our model easily satisfies this condition.

elements such as Eu have been discovered (see McWilliam et al. 1995). This means that r -process nucleosynthesis must happen on the same timescale as Fe production in supernovae.

Standard explosive nucleosynthesis in core-collapse supernovae can produce only the lighter r -process elements with mass number $A < 130$, such as Rh and Ag. Some other mechanism is needed to produce the heavier r -process elements with $A > 130$. Moreover, this mechanism should not produce too much light r -process elements. If it did, we would have difficulty explaining the fact that, among metal poor stars, there is a variation of the abundance of the heavier r -process elements with $A > 130$ whereas the abundances of the elements from O to Ge and the lighter r -process elements up to Ag are unchanged (Qian 2005). In standard models of core-collapsed supernovae, neutron rich regions suitable for r -process synthesis do exist, but the problem is that these regions generally do not flow out but rather fall back on the proto-neutron star. Although the possibility that a neutrino driven wind may eject the neutron rich region has been studied, at least one of the following conditions has to be satisfied: (i) low lepton fraction Y_e , (ii) short dynamical timescale, and (iii) large entropy per baryon. To our knowledge, these conditions have not been achieved naturally in supernova wind models (Hoffman, Woosley & Qian 1997)¹⁰.

Another idea that has been considered by some workers is accretion-induced collapse (AIC) as a candidate site for r -process nucleosynthesis (Qian & Wasserburg 2002). It is reported that this scenario produces heavier elements with $A > 130$ without overproducing the lighter elements. We cannot judge whether or not the necessary conditions are naturally realized.

In comparison to these other models, the disk wind model we propose here appears to be plausible and quite natural. The main selling point of this model is that we can easily bring the neutron rich material and r -process elements out during the core-collapse supernova explosion.

4. Summary and Discussion

In this paper we have shown that, if an accretion disk — an NDAF — forms around a proto-neutron star during core collapse of a massive progenitor star, then a substantial

¹⁰Some attempts have been made to resolve the above difficulties making use of special assumptions, e.g., neutrino oscillations between active and sterile neutrinos (Fetter et al. 2003 and references therein), jet-like MHD explosion (Nishimura et al. 2005) for a lower lepton fraction, general relativistic effect for a shorter dynamical timescale (Otsuki et al. 2000), quantum electrodynamical effect in the strong magnetic field for a larger entropy per baryon (Kohri, Yamada & Nagataki 2004), and so on.

quantity of mass is likely to be ejected from the disk and to carry with it a large amount of mechanical energy. The outflow energy could be as much as 10^{51} erg in favorable situations and might be sufficient to convert a failed supernova explosion into a successful one. A virtue of this proposal is that essentially all the energy is available to power the explosion. This is in contrast to neutrino-driven supernovae where only a small fraction of the energy is deposited in the stellar mantle.

We have estimated the energy in the outflow corresponding to two distinct scenarios. In one scenario (§ 3.3, Fig. 10), we assume that the disk forms as part of the initial core collapse and that the outflow induces a prompt supernova explosion. In the second scenario (§ 3.4, Fig. 11), we assume that there is no prompt explosion and that the shock stalls. However, some of the subsequent fallback material forms a disk whose outflowing wind re-energizes the shock and causes a delayed supernova explosion.

Depending on the parameters we assume, primarily the amount of mass available in the disk, both the above scenarios are feasible for producing a supernova explosion. However, the second scenario (which leads to a delayed explosion) appears to be more promising for two reasons. First, the total amount of fallback mass in a failed supernova can be several solar masses (essentially all the mass in the envelope of the progenitor star) whereas the mass in the initial prompt disk is likely to be no more than a few tenths of a solar mass. Thus, the mass and energy budget is much larger in the delayed scenario. Second, the delayed fallback material is likely to have larger specific angular momentum since it originates from farther out in the progenitor star. Thus, this material is more likely to form a disk.

The results shown in Figures 10 and 11 are conservative in that they do not include the additional energy that is released when the dissociated nucleons in the outflowing gas recombine to form larger nuclei. The latter process releases about 8 MeV per nucleon (MacFadyen 2003) which can be a substantial fraction of the total outflow energy for certain parameter choices. Figure 12 shows how the results shown in Figure 8 are modified when the recombination energy is included. The difference is quite large, especially when the energy efficiency factor ξ of the outflow is small, say ~ 0.1 . This makes the scenario proposed in this paper even more promising.

Although we have taken pains to model the physics of the NDAF in as much detail as possible, the numerical results we have obtained are still only crude estimates. This is because there are several large uncertainties in the model which we have had to absorb in various free parameters. In both the prompt and delayed scenarios, we have no firm estimate of how much mass goes into the disk. The mass depends on the angular momentum distribution of the progenitor star, which is poorly understood. Also, we do not know how much of the mass in the disk flows out in the wind. While it is generally understood that

advection-dominated accretion flows are likely to have strong outflows (Narayan & Yi 1994, 1995a), the exact amount of outflow is uncertain. We have included an index s_0 plus an approximate prescription for how the index varies with the degree of advection-domination in the accretion flow (see eq. (66)). Finally, we do not have a precise estimate of the specific energy of the outflowing gas. We make the plausible assumption that the energy is a fraction $\xi < 1$ of the escape energy, but there are no strong constraints on the value of ξ .

Despite these large uncertainties, we believe our calculations are realistic enough to demonstrate that there is likely to be considerable energy in the outflow. One question to ask is: Where exactly does the energy come from? The responsible agency is gravity, helped by viscosity (or more accurately shear stress in the accretion flow). As is well-known (e.g., Frank et al. 1992), viscosity has three important effects on an accretion flow.

(i) Viscosity induces a shear stress which transports angular momentum outward, enabling mass to flow in. This is obviously critical for the whole accretion process to occur in the first place. The “viscosity” is likely to be generated via the magnetorotational instability (Balbus & Hawley 1991).

(ii) Viscous dissipation heats up the gas locally. If this heat is radiated immediately, then the gas remains cold and its binding energy is approximately $GM/2R$ (in the Newtonian limit), i.e., it is equal to half the local potential energy. Such highly bound gas is not easily ejected and we do not expect a significant wind from the disk. However, if the heat energy is not radiated, i.e., if the flow is advection-dominated, then the gas is much more loosely bound to the central mass; in fact, the gas is actually unbound as we discuss below in (iii). An ADAF is thus expected to have heavy mass loss, as originally highlighted by Narayan & Yi (1994, 1995a).

(iii) Finally, viscosity transports energy outward. The outward energy flux is given by $F_{\text{out}} = T_{r\phi}\Omega$, where $T_{r\phi}$ is the local shear stress (which transports angular momentum outward) and Ω is the local angular velocity of the gas. In the case of an ADAF, this outward transport of energy is extremely important. As we discussed above in (ii), the gas in an ADAF does not lose any of its initial binding energy because it is radiatively inefficient. Now, we see that, in addition, it acquires extra energy from gas further in through viscous energy transport. The net result is that the gas in an ADAF ends up with *positive* energy (or negative binding energy). Narayan & Yi (1994, 1995a) explicitly demonstrated this by estimating the Bernoulli parameter of the gas and showing that this quantity is positive for a self-similar ADAF. The positive energy drives the outflow and deposits energy in the surroundings. Where does the energy come from? Ultimately, it comes from the gravitational potential energy released by the gas that falls onto the compact star on the inside.

The above discussion establishes the strong connection between advection-dominated accretion and outflowing winds. Therefore, the mechanism we have described will not operate unless the accretion flow is strongly advection-dominated. Fortunately, ADAF-like conditions are present over a wide range of parameter space in an NDAF (see Fig. 3). Equally, the mechanism will not operate in a numerical simulation of a supernova explosion unless one includes viscosity self-consistently and keeps track of the energy that is transported and dissipated viscously.

To the best of our knowledge, viscous interactions have not been properly incorporated in most supernova simulations done so far. An exception to this statement is the work of Fryer & Heger (2000) which investigated rotating collapse with the inclusion of α -viscosity. While there is some evidence for outflowing gas in their simulation (see their Fig. 14), nevertheless, the energy carried by the wind is apparently not very important because the authors find that the supernova explosion develops more slowly in a rotating star compared to a non-rotating star. Without knowing all the details of the simulation, it is difficult to say why this work did not find the energetic wind that we predict. Values of α over the range 0.1 to 0.0001 were apparently used and this may be a clue. Comparing Figures 8 and 9 of the present paper, we see that when α is reduced from 0.1 to 0.01, the range of \dot{M} over which the wind is relatively inefficient (because the accretion flow is relatively efficient at radiating neutrinos) increases substantially. The reason for this is explained in § 3.2. For yet smaller values of α such as those mentioned in Fryer & Heger (2000), the effect would be even more enhanced. It is thus possible that the viscosity employed by Fryer & Heger (2000) was too weak to exhibit the effects we have described. It is also possible that the progenitors they used did not rotate fast enough to develop a substantial accretion disk around the proto neutron star.

Regardless, once three-dimensional simulations of rotating collapse are done with full MHD (so that the magnetorotational instability is able to develop and provide “viscosity” self-consistently), the effects we have described in this paper ought to be seen. The work of Proga et al. (2003) and Moseenko et al. (2005) is a beginning in this direction.

It should be noted that the outflows we consider here are distinct from the relativistic jets that are popular in collapsar models of gamma-ray bursts (MacFadyen & Woosley 1999) or that are invoked in some models of supernovae (Wheeler et al. 2002). Our outflows are relatively slow. Even the gas that is ejected from the innermost region of the disk has a speed only $\sim 0.2c$ (its kinetic energy is $\xi GM/R_{\text{in}}$); the gas that comes out from larger radii is even slower. Also, we do not expect the outflow to be highly collimated as visualized in jet models. In our view, if at all an ultrarelativistic jet is present, it is likely to be produced by some mechanism that is completely different from the disk outflow we have considered.

The mechanism will probably be related to the compact object in the middle and not the disk. Of course, a fraction of the jet energy may contribute to re-energizing the stalled shock (Wheeler et al. 2002) and may assist the disk outflow in producing the explosion. Equally, the disk outflow that we discuss here may help, or even play an important role, in the collimation of the relativistic jet.

An important point to note is that the outflow discussed in this paper has a clear direction associated with it, namely the rotation axis of the system. The impact of this non-spherical wind on the stalled shock is likely to result in an asymmetric explosion for which there is growing evidence from polarization observations of supernovae (Wheeler et al., 2000; Wang et al., 2001).

Finally, we note that several regions in the disk have a large neutron to proton ratio. Because of the short dynamical timescale, these neutron-rich regions are candidate sites for r -process nucleosynthesis. In our model, the neutron-rich gas and the r -process elements that it synthesizes are naturally transported out by the outflow and ejected in the supernova explosion. The model may thus be of interest for studies of the origin of r -process elements in the universe (Pruet et al. 2003, 2004a,b; Fujimoto et al. 2004; Surman & McLaughlin 2004, 2005).

Acknowledgements

We wish to thank E. Livne for providing unpublished results from core collapse simulations, and the anonymous referee for helpful comments. K.K. also thanks R. Sawyer, Shoichi Yamada and M. Yokosawa for useful discussions. This work was supported in part by NASA grant NAG5-10780, NSF grant AST-0307433, JSPS Research Fellowships 15-03605 and US-Israel BSF grant.

A. Appendix: Reaction rates and various timescales

Here we compare the timescale of the various scattering processes with the dynamical timescale in the system. The dynamical timescale is represented by the accretion time,

$$t_{\text{acc}} \equiv \frac{1}{\alpha} \sqrt{\frac{R^3}{GM_{\text{BH}}}} \left(\frac{R}{H}\right)^2. \quad (\text{A1})$$

For reference, if we simply assume that the disk half-thickness is $H \sim R/2$ (as appropriate for an ADAF), then the dynamical timescale is approximately given by $t_{\text{acc}} \simeq 3.0 \times 10^{-2} \text{ s} (\alpha/0.1)^{-1} (R/7R_{\text{S}})^{3/2} (M_{\text{BH}}/3M_{\odot})$.

The timescale of the scattering rates among photons and electrons is much faster than the accretion timescale because of the electromagnetic interaction (Thomson scattering), i.e., $t_{\gamma e} \sim 1/(\sigma_{\text{T}} n_{\gamma} c) \sim 10^{-18} T_{11}^{-3} \text{ s}$, with Thomson cross section σ_{T} . Therefore, we obviously expect that photons and electrons interact each other rapidly and are immediately thermalized.

On the other hand, neutrinos with energy $\sim k_{\text{B}}T$ scatter off the background nucleons and electrons only through the weak interaction. The reaction rates of these scattering processes are roughly estimated by

$$\Gamma_{\nu e} \sim \Gamma_{\nu N} \sim G_{\text{F}}^2 (k_{\text{B}}T)^2 n_e. \quad (\text{A2})$$

Note that this rate is of the same order of magnitude as that of neutrino-antineutrino pair production by background electron-positron annihilation $\Gamma_{e^+e^- \rightarrow \nu\bar{\nu}}$. Thus, the timescale of scattering (or the pair-production) is $t_{\nu e} \sim t_{\nu N} \sim t_{e^+e^- \rightarrow \nu\bar{\nu}} \sim [G_{\text{F}}^2 (k_{\text{B}}T)^2 n_e]^{-1}$. The condition $t_{\nu e} \ll t_{\text{acc}}$, i.e., $\Gamma_{\nu e}/t_{\text{acc}}^{-1} \gg 1$ approximately means that neutrinos can scatter off background particles and transfer their energy to them within a typical dynamical timescale. In Fig. 13 (a) we plot contours of the ratio $\Gamma_{\nu e}/t_{\text{acc}}^{-1}$. We find that neutrinos scatter off background particles efficiently in the upper left region. However, please note that in terms of the thermalization of neutrinos, $\Gamma_{\nu e}/t_{\text{acc}}^{-1} \gg 1$ is just a necessary condition, not a sufficient condition. In this study we conservatively regard the ν_i 's to be thermalized only when both $\tau_{a,\nu_i} \gg 1$ and $\tau_{s,\nu_i} \gg 1$ are satisfied. As shown in Figs. 5 (a) and (b), the parameter region where both conditions are satisfied is surely included in the region where $\Gamma_{\nu e}/t_{\text{acc}}^{-1} \gg 1$ in Fig. 13 (a).

It is also useful to discuss the timescale of the interconverting rates between neutrons and protons through the weak interaction. The expressions of the rates are presented in Eqs. (23) – (28). In particular, electron capture by a proton and positron capture by a neutron are important to interconvert neutrons and protons in the electromagnetic thermal

bath. This is because these processes are effective even when the neutrino-nucleon scattering in Eqs. (26) – (28) is ineffective due to insufficient thermalization of background neutrinos. We plot contours of the ratio $\Gamma_{pe^- \rightarrow n\nu_e}/t_{\text{acc}}^{-1}$ in Fig. 13 (b). From the condition $\Gamma_{pe^- \rightarrow n\nu_e}/t_{\text{acc}}^{-1} \gg 1$ (which is the same as $(n/p) \times \Gamma_{ne^+ \rightarrow p\bar{\nu}_e}/t_{\text{acc}}^{-1} \gg 1$ in thermal equilibrium of n/p), we see that the electron-capture processes by nucleons are effective in the upper left region of the r - \dot{m} plane.

B. Appendix: Actual calculation of n/p

Here we discuss the approximations we use to calculate the neutron to proton ratio n/p in this study. Ideally, we should solve the balance equation of the interconverting reactions between neutrons and protons written down in Eqs. (21) and (22). However, let us make some bold but reasonable approximations since the exact calculations require intensive computations and are not needed for our current purpose.

We classify the r - \dot{m} plane into following three regions: (i) the region where neutrinos are completely thermalized and the timescale for the interconverting reaction $\Gamma_{n \leftrightarrow p}$ is much smaller than the dynamical timescale, (ii) the region where $\Gamma_{n \leftrightarrow p}$ is rapid but the thermalization of neutrinos is incomplete and the neutrino-nucleon scattering is unimportant, and (iii) the region where $\Gamma_{n \leftrightarrow p}$ is slow compared to the dynamical timescale. We discuss each of the three cases in detail.

First of all, it is necessary to know the distribution functions of electrons and neutrinos, which govern the balance equations of the interconverting reactions. As we have discussed in Appendix A, the thermalization of electrons is easily realized because the electromagnetic interaction is very rapid compared to the dynamical timescale.

On the other hand the thermalization of neutrinos is not obvious. The problem is that neutrinos scatter off the background particles such as electrons, nucleons or neutrinos only through the weak interaction. For accurate results, we would have to solve a set of the Boltzmann equations to trace the time evolution of the energy-distribution function of neutrinos and their energy transfer. Instead, for simplicity, we adopt the following approximate method which does not involve explicitly solving the Boltzmann equations. When both τ_{a,ν_i} and τ_{s,ν_i} are much larger than $2/3$, it is reasonable to expect that neutrinos are completely thermalized, so we assume this. The corresponding parameter regime is clearly shown in Figs. 5(a) and (b) for the electron neutrinos. In addition, from Fig. 13 (a), we see that the timescale of such scatterings through νe (νN , and $\nu\nu$) is much more rapid than the dynamical timescale. Therefore, as shown in Eq. (30), we obtain $n/p = \exp(-Q/k_B T + \eta_e)$

as the thermal equilibrium value of the neutron to proton ratio (case (i)).

If the electron neutrinos are not thermalized, i.e., if the optical depths τ_{a,ν_e} and τ_{s,ν_e} are less than $2/3$ in the current context, it would be reasonable to regard that the neutrino-nucleon scatterings in Eqs. (26), (27) and (28), are not important and can be ignored, compared with the other processes in Eqs. (23), (24) and (25). In Fig. 13 (b) we find the parameter regions where the condition $\Gamma_{pe^- \rightarrow n\nu_e}/t_{\text{acc}}^{-1} \gg 1$, i.e., $(n/p)\Gamma_{ne^+ \rightarrow n\nu_e}/t_{\text{acc}}^{-1} \gg 1$ is realized, while τ_{a,ν_e} and τ_{s,ν_e} are less than $2/3$. In this region, we approximately have $n/p \simeq (\Gamma_{pe^- \rightarrow n\nu_e})/(\Gamma_{ne^+ \rightarrow p\bar{\nu}_e} + \Gamma_{n \rightarrow pe^- \bar{\nu}_e})$ as the equilibrium value with $f_{\nu_e} \sim f_{\bar{\nu}_e} \sim 0$ (case (ii)).

Finally, if the timescale of the above interconverting reactions is not shorter than the accretion time, $\Gamma_{p \leftrightarrow n}/t_{\text{acc}}^{-1} < 1$, we can no longer expect any kind of equilibrium to be achieved in the neutron to proton ratio through the weak interaction. In this case, we assume that the neutron to proton ratio approximately becomes unity ($n/p \simeq 1$). This is a reasonable assumption because most of the free nucleons are produced by the destruction (e.g., through the photodissociation) of heavy nuclei such as He, C, N and O, which contain approximately equal numbers of neutrons and protons (case (iii)).

In Fig. 14, we show the neutron to proton ratio as a function of the temperature in units of 10^{11} K for representative examples of cases (i) and (ii). The dotted lines denote case (i) in which electron neutrinos are completely thermalized and the neutrino-nucleon collisions are important, i.e., $n/p = \exp(-Q/k_B T + \eta_e)$. The solid lines denote case (ii) in which we omit the neutrino-nucleon collisions and $n/p = \Gamma_{pe^- \rightarrow n\nu_e}/(\Gamma_{ne^+ \rightarrow p\bar{\nu}_e} + \Gamma_{n \rightarrow pe^- \bar{\nu}_e})$. The upper (lower) lines correspond to $\eta_e = 1$ ($\eta_e = 10^{-3}$).

In Fig. 6 (b), we plot contours of the neutron to proton ratio n/p in the $r-\dot{m}$ plane. We see that n/p becomes greater than unity in the upper left region. This is typical for the equilibrium value of n/p for a positive finite η_e . Neutron rich material flowing out of this region could experience r -process nucleosynthesis as we discuss in § 3.5 and 4.

REFERENCES

- Abramowicz, M.A., Igumenshchev, I.V., Lasota, J.-P. 1998, MNRAS, 293, 443
- Arnett, D. 1967, Can. J. Phys. 45, 1621
- Balbus, S. A., & Hawley, J. F. 1991, ApJ, 376, 214
- Bethe, H. A., & Wilson, J. R. 1985, ApJ, 295, 14
- Blandford, R. D., & Begelman, M. C. 1999, MNRAS, 303, L1
- Bruenn, S. W. 1985, ApJS, 58, 771
- Bruenn, S. W., & Mezzacappa, A. 1997, Phys. Rev., D56, 7529.
- Bruenn, S. W., De Nisco, K. R., & Mezzacappa, A. 2001, ApJ, 560, 320
- Burrows A., & Goshy J. 1993, ApJL, 416, L75
- Burros, A., Hayes, J.,m & Fryxell, B. A. 1995, ApJ, 450, 830
- Burrows A., & Thompson, T. 2002, in From Twilight to Highlight: The Physics of Supernovae, held in Garching bei München, Germany, July 29-31, 2002, eds. Bruno Leibundgut and Wolfgang Hillebrandt (astro-ph/0210212)
- Burrows, A., Young, T., Pinto, P., Eastman, R., & Thompson, T.A. 2000, ApJ, 539, 865
- Colgate. S., & White R. H. 1996, ApJ, 143, 626
- Di Matteo, T., Perna R., & Narayan, R. 2002, ApJ, 579 706
- Eichler, D., Livio, M., Piran, T., & Schramm, D. N. 1989, Nature, 340, 126
- Eidelman, S. et al., Particle Data Group collaboration 2004, Phys. Lett., B592, 1
- Fetter, J., McLaughlin, G.C., Balantekin, A.B. & Fuller, G.M. 2003, Astropart. Phys., 18, 433
- Frank, J., King, A., Raine, D. 1992, *Accretion Power in Astrophysics*, 2nd ed., Cambridge University Press, Cambridge
- Freiburghaus, C., Rosswog, S., & Thielemann, F.-K. 1999, ApJ, 525, L121
- Fryer, C. L. 1999, ApJ, 522, 413

- Fryer et al. 1999 ApJ, 516, 892
- Fryer, C. L., & Heger, A. 2000, ApJ, 541, 1033
- Fryer, C. L., & Warren, M. S. 2002, ApJ, 574, L65
- Fryer, C. L., & Warren, M. S. 2004, ApJ, 601, 391
- Fujimoto, S., Hashimoto, M., Arai, K., & Matsuba, R. 2004, ApJ, 614, 847
- Goodman, J., Dar, A., & Nussinov, S. 1987, ApJ, 314, L7
- Hannestad, S. & Raffelt, G. 1998, ApJ, 507, 339
- Heger, A., Langer, N., & Woosley, S. E. 2000, ApJ, 528, 368
- Heger, A., Woosley, S. E., & Spruit, H. C. 2004, ArXiv Astrophysics e-prints, astro-ph/0409422
- Herant, M., et al. 1994, ApJ, 435, 339
- Hoffman, R.D., Woosley, S.E. & Qian, Y.-Z. 1997, ApJ, 482, 951
- Igumenshchev et al. 2000, ApJ, 537, L27
- . 2003, ApJ in press, astro-ph/0304125
- Janka, H. T., & Muller, E. 1996, A&A, 306, 167
- Janka, H. T., Scheck, L., Kifonidis, K., Mueller, E., & Plewa, T. 2004, ArXiv Astrophysics e-prints, astro-ph/0408439
- Kohri, K., & Mineshige, S. 2002, ApJ, 577 311
- Kohri, K., Yamada, S. & Nagataki, S. 2004, Astropart. Phys., 21, 433
- Kotake, K., Sawai, H., Yamada, S., & Sato, K. 2004, ApJ, 608, 391
- Kotake, K., Yamada, S., & Sato, K. 2003, ApJ, 595, 304
- Latimer, J. M., & Prakash, M. 2004, Science, 304, 536
- Leblanc, J. M., & Wilson, J. R. 1970, ApJ, 161, 541
- Lee, W. H., Ramirez-Ruiz, E., & Page, D. 2004, ApJ, 608, L5
- Liebendorfer, et al. 2001, Phys Rev. D63, 103004

- Liebendorfer, M., Rampp, M., Janka, H.-Th., & Mezzacappa, A. 2005, ApJ, in press (astro-ph/0310662)
- Livne, E., private communication
- Livne, E., Burrows, A., Walder, R., Lichtenstadt, I., & Thompson, T. A. 2004, ApJ, 609, 277
- Mezzacappa, A., et al. 2001, Phys. Rev. Lett., 86, 1935
- Mineshige, S., Nomura, H., Hirose, M., Nomoto, K., & Suzuki, T. 1997, ApJ, 489, 227
- Moiseenko, S. G., Bisnovatyi-Kogan, G. S., & Ardeljan, N. V. 2003, Revista Mexicana de Astronomia y Astrofisica, 15, 231
- Myra, E. S., & Burrows, A. 1990, ApJ, 364, 22
- MacFadyen, A.I. 2003, astro-ph/0301425
- MacFadyen, A.I., & Woosley, S.E. 1999, ApJ, 524, 262
- McWilliam, A., et al. 1995, AJ, 109, 2757
- Narayan, R., Mahadevan, R., & Quataert, E. 1998, in Theory of Black Hole Accretion, Eds M. A. Abramowicz, G. Bjornsson, and J. E. Pringle, p148, Cambridge Univ. Press
- Narayan, R., Piran, T., & Kumar, P. 2001, ApJ, 557, 949
- Narayan, R., & Yi, I. 1994, ApJ, 428, L13
- 1995a, ApJ, 444, 231
- 1995b, ApJ, 452, 710
- Nishimura, S., et al. 2004, astro-ph/0504100
- Otsuki, K., Tagoshi, H., Kajino, T. & Wanajo, S. 2000, ApJ, 533, 424
- Pen, U.-L. 2003, ApJ, 596, L207
- Popham, R., & Narayan, R. 1995, ApJ, 442, 337
- Popham, R., Woosley, S.E., & Fryer, C. 1999, ApJ, 518, 356
- Proga, D., MacFadyen, A. I., Armitage, P. J., & Begelman, M. C. 2003, ApJ, 599, L5

- Pruet, J., Surman, R., & McLaughlin, G. C. 2004, ApJ, 602, L101
- Pruet, J., Thompson, T. A., & Hoffman, R. D. 2004, ApJ, 606, 1006
- Pruet, J., Woosley, S. E., & Hoffman, R. D. 2003, ApJ, 586, 1254
- Qian, Y.-Z. 2005, astro-ph/0501235
- Qian, Y.-Z., & Wasserburg G.J. 2002, ApJ, 588, 1099
- Qian, Y.-Z. & Woosley, S.E. 1996, ApJ, 471, 331
- Rampp M., & Janka, H. T. 2000, ApJL, 539, 33
- Ruffert, M., Janka, H.-Th. & Schäfer 1996, A&A, 311, 532
- Scheck, L., Plewa, T., Janka, H.-T., Kifonidis, K., & Mueller, E. 2004, Phys. Rev. Lett., 92, 011103
- Shapiro, S. L., & Teukolsky, S. A. 1983, in “*Black Holes, White Dwarfs and Neutron Stars*,” eds by John Wiley & Sons, Inc: Chapter 18
- Shinder, P.J., Schramm, D.N., Wiita, P.J., Margolis, S.H. & Tubbs, D.L. 1987, ApJ, 313, 531
- Surman, R., & McLaughlin, G. C. 2004, ApJ, 603, 611
- Surman, R., & McLaughlin, G. C. 2005, ApJ, 618, 397
- Thompson, T. A., Burrows, A., & Meyer, B. S. 2001, ApJ, 562, 887
- Thompson, T. A., Burrows, A., & Pinto, P. A. 2003, ApJ, 592, 434
- Thompson, T. A., Quataert, E., & Burrows, A. 2005, ApJ, in press (astro-ph/0403224)
- Tubbs, D., & Schramm, D. N. 1975, ApJ, 201, 467
- Walder, R., Burrows, A., Ott, C. D., Livne, E., Lichtenstadt, I., & Jarrah, M. 2004, ArXiv Astrophysics e-prints, astro-ph/0412187
- Wang, L., Howell, D. A., Höflich, P., & Wheeler, J. C. 2001, ApJ, 550, 1030
- Wheeler, J. C., Meier, D. L., & Wilson, J. R. 2002, ApJ, 568, 807
- Wheeler, J. C., Yi, I., Höflich, P., & Wang, L. 2000, ApJ, 537, 810

- Wilson, J. R. 1985, in Numerical Astrophysics, Ed. Centrella., LeBlanc J. M., & Bowers R. L., p 442. Boston (Jones & Bartlett Publ)
- Woosley, S.E., & Baron, E. 1992, ApJ, 391, 228
- Yokosawa, M., Uematsu, S., & Abe J. 1005, astro-ph/0412558
- Yuan, F., Cui, W., & Narayan, R. 2004, ApJ, in press (astro-ph/0407612)
- Yuan, F., Quataert, E., & Narayan, R. 2003, ApJ, 598, 301

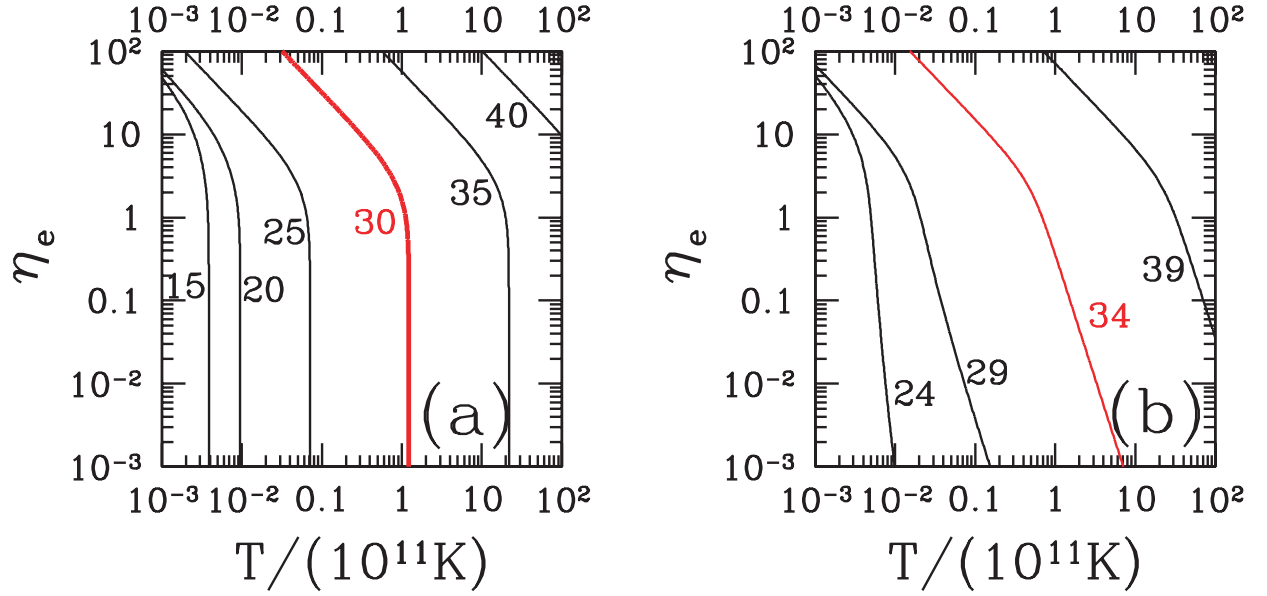


Fig. 1.— (a) Contours of the total pressure of electrons and positrons, $p_e \equiv p_{e-} + p_{e+}$ (eqs. 13–15), in the T - η_e plane. The contours are labeled by the value of $\log_{10}[p_e/(\text{erg cm}^{-3})]$. (b) Contours of the net number density of electrons, $n_e \equiv n_{e-} - n_{e+}$ (eqs. 18–20), in the T - η_e plane. The contours are labeled by the value of $\log_{10}[n_e/(\text{cm}^{-3})]$.

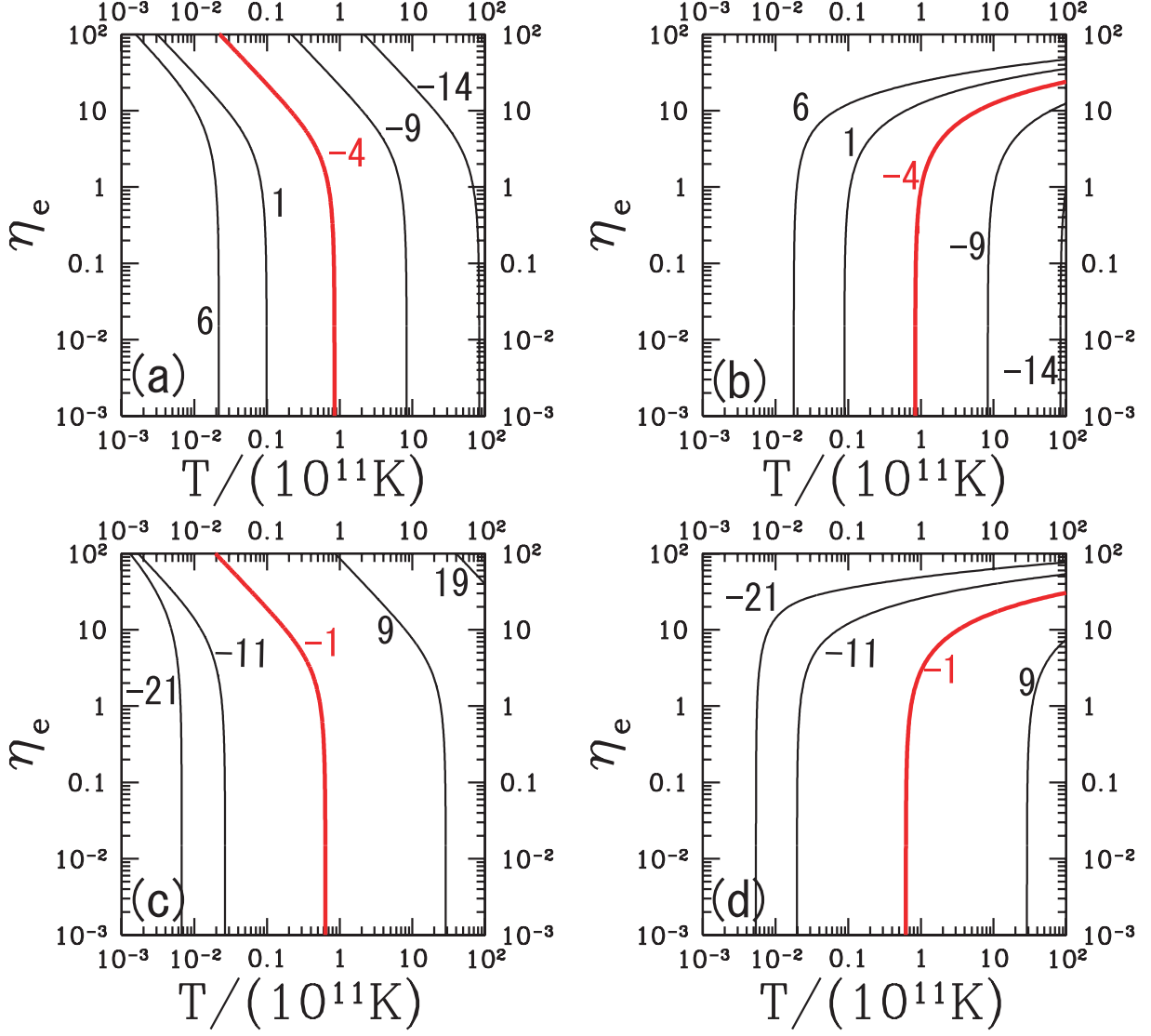


Fig. 2.— (a) Contours of the proton to neutron conversion timescale $\log_{10}[\Gamma_{pe^- \rightarrow n\nu_e}^{-1}/\text{s}]$ (eq. 24). (b) Same as (a), but for the neutron to proton reaction timescale $\Gamma_{ne^+ \rightarrow p\nu_e}^{-1}$ (eq. 23). (c) Contours of the neutrino-cooling rate $\log_{10}[q_{pe^- \rightarrow n\nu_e}^-/n_p/(\text{erg s}^{-1})]$ (eq. 48) in the T - η_e plane. (d) Same as (c), but for the rate $\log_{10}[q_{ne^+ \rightarrow p\nu_e}^-/n_n/(\text{erg s}^{-1})]$ (eq. 49).

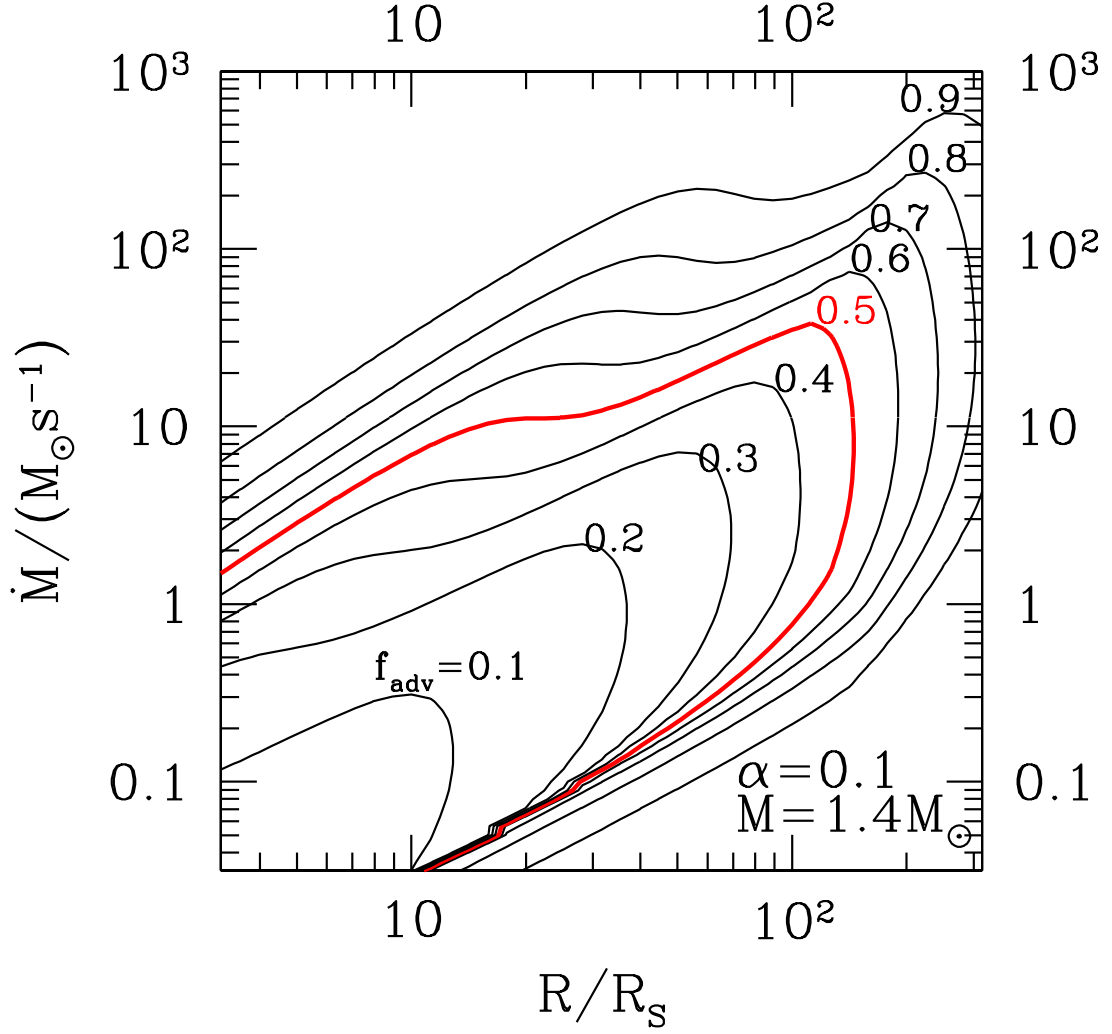


Fig. 3.— Contours of the advection parameter $f_{\text{adv}} \equiv Q_{\text{adv}}^-/Q^+$ in the r - \dot{m} plane, where $r \equiv R/R_s$ and $\dot{m} \equiv \dot{M}/M_\odot \text{s}^{-1}$. The parameter f_{adv} is a measure of the disk thickness (see eq. 46) and also determines how susceptible the disk is to producing an outflow (§§ 3.1, 3.2). The results shown correspond to a viscosity parameter $\alpha = 0.1$ and a compact central object of mass $M = 1.4 M_\odot$.

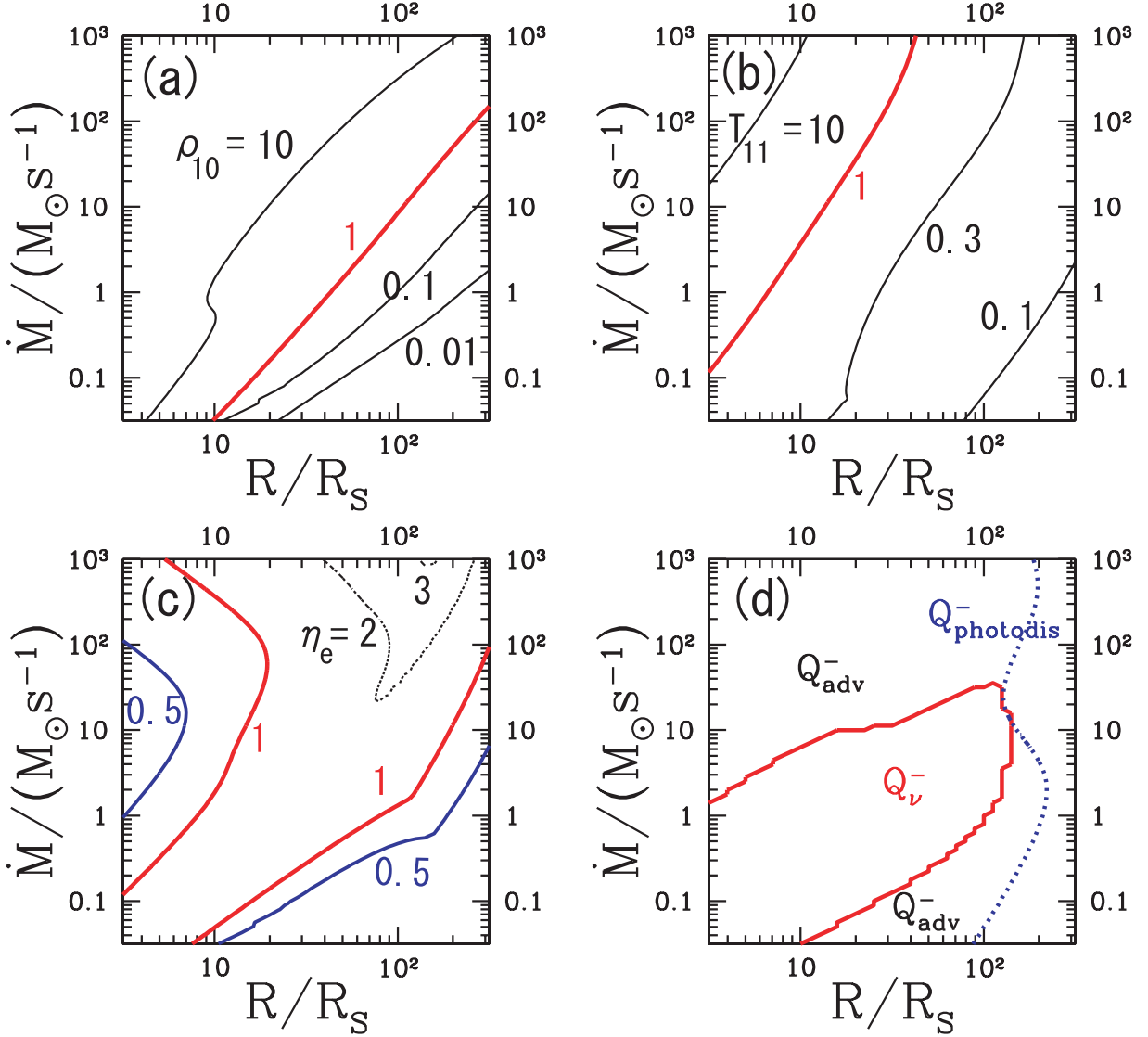


Fig. 4.— (a) Contours of the matter density $\rho_{10} = \rho/10^{10} \text{ g cm}^{-3}$ in the r - \dot{m} plane. The thick solid line corresponds to $\rho_{10} = 1$. (b) Contours of $T_{11} = T/10^{11} \text{ K}$. (c) Contours of η_e . Note that η_e becomes large toward the upper right region. (d) Dominant cooling process in various regions of the r - \dot{m} plane. In the central region, neutrino cooling Q_ν^- dominates, with electron-positron capture being the most important process. In the region on the right, photodissociation of nuclei is important. The dotted line shows the contour corresponding to mass fraction of nucleons $X_{\text{nuc}} = 0.5$, where most nuclei are destroyed by endothermic photodissociation (see Fig. 6(a) and the discussion in Section 2.3.2). Advective cooling dominates in the rest of the plane, as seen also in Fig. 3. All panels correspond to $\alpha = 0.1$ and $M = 1.4M_\odot$.

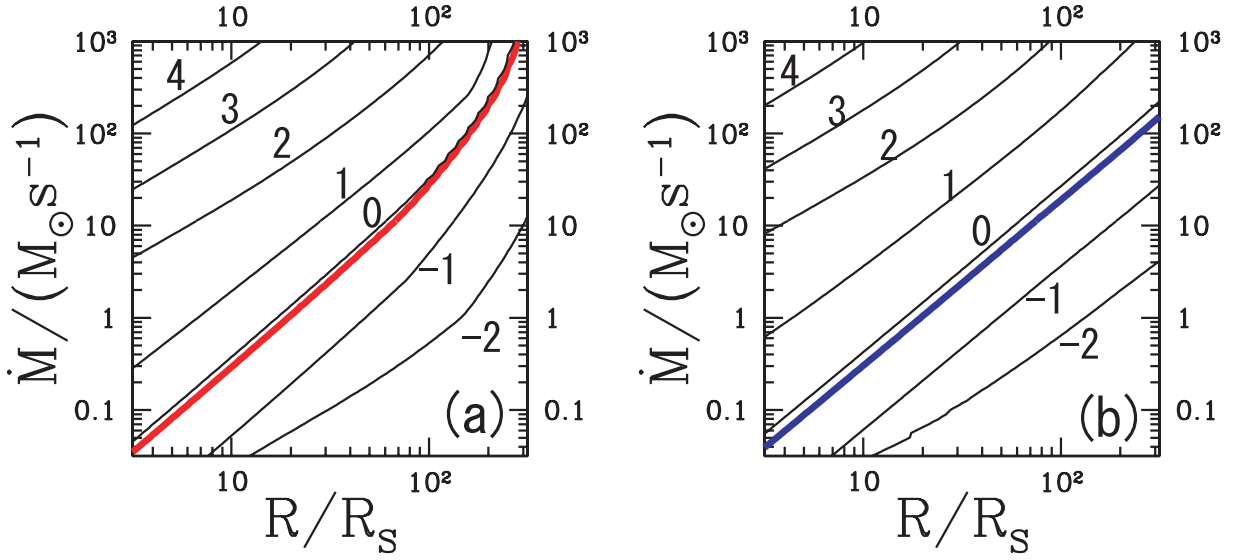


Fig. 5.— (a) Contours of the neutrino absorption optical depth $\log_{10}(\tau_{a,\nu_e})$ in the r – \dot{m} plane. The thick solid line corresponds to $\tau_{a,\nu_e} = 2/3$. (b) Contours of the neutrino scattering optical depth $\log_{10}(\tau_{s,\nu_e})$. The results are for $\alpha = 0.1$ and $M = 1.4M_\odot$.

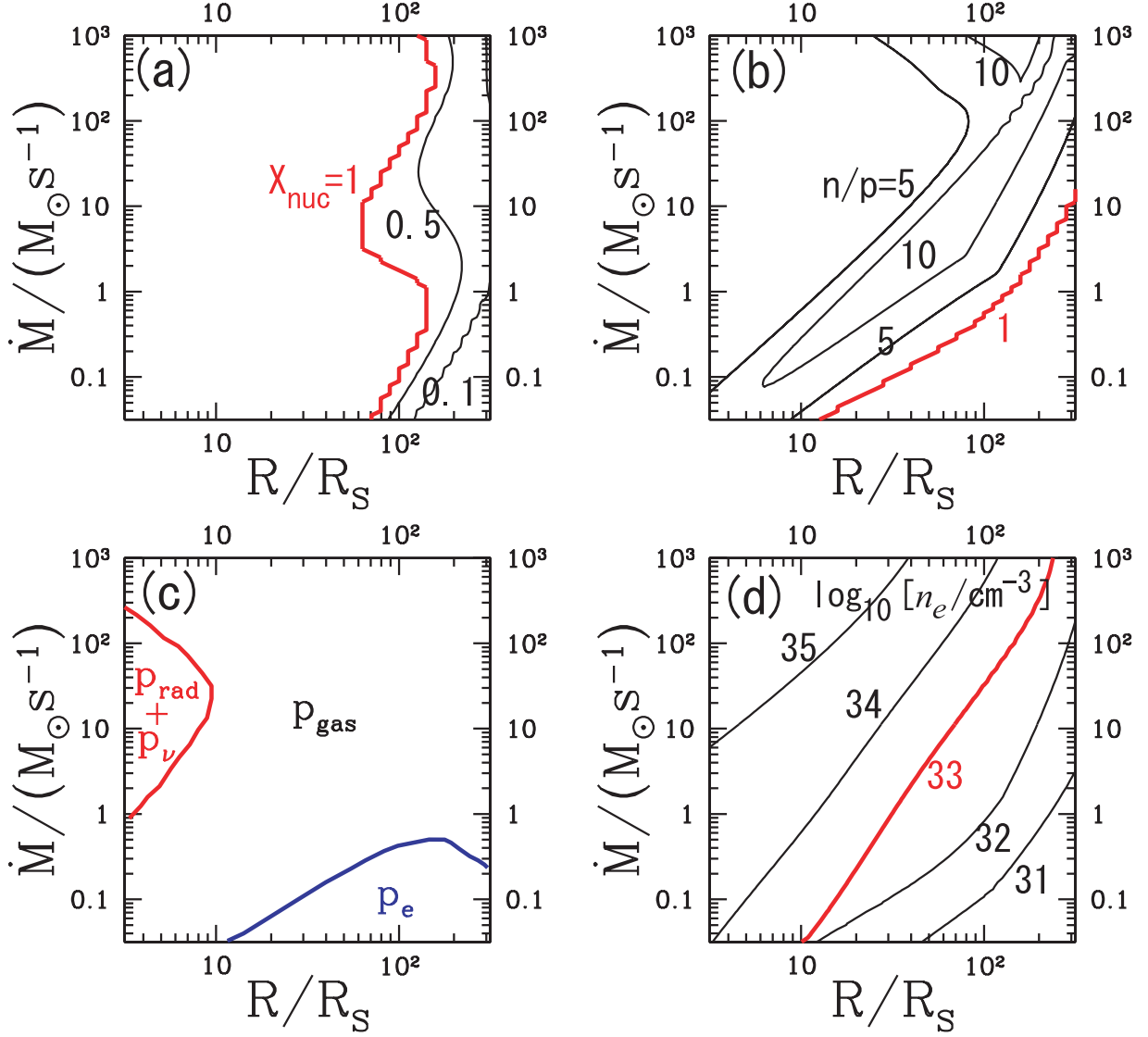


Fig. 6.— (a) Contours of the nucleon fraction X_{nuc} in the r - \dot{m} plane. For $r \lesssim 150$, the region of most interest to us, we have $X_{\text{nuc}} \sim 1$, i.e., the nuclei are completely destroyed into free nucleons. (b) Contours of the neutron to proton ratio n/p . (c) The dominant source of pressure in different regions of the r - \dot{m} plane. (d) Contours of the number density of electrons $\log_{10}[n_e/\text{cm}^{-3}]$. All results are for $\alpha = 0.1$ and $M = 1.4M_\odot$.

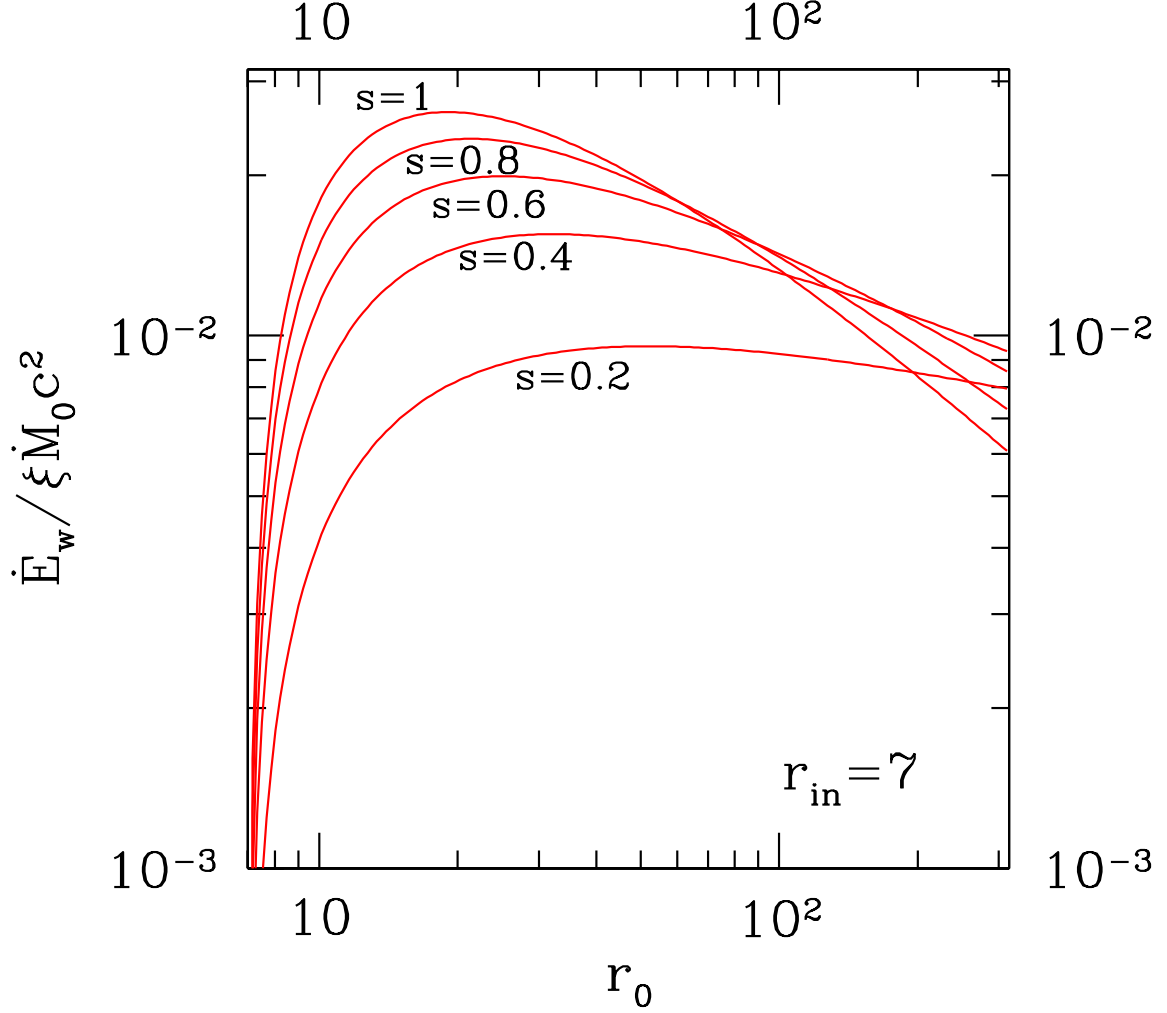


Fig. 7.— Approximate analytical estimate of the energy available in the wind from a fully advection-dominated accretion flow. \dot{E}_w is the power in the wind and $\dot{M}_0 c^2$ is the rate at which rest mass energy is supplied to the disk at its outer radius R_0 . The ratio of these quantities measures the outflow efficiency and is plotted along the ordinate. The index s describes how much mass is lost in the outflow and ξ measures the specific energy of the outflowing gas. The inner edge of the accretion flow is taken to be at $r_{\text{in}} = 7$, which corresponds to ~ 30 km for a $1.4M_\odot$ compact object. (See § 3.1 for details.)

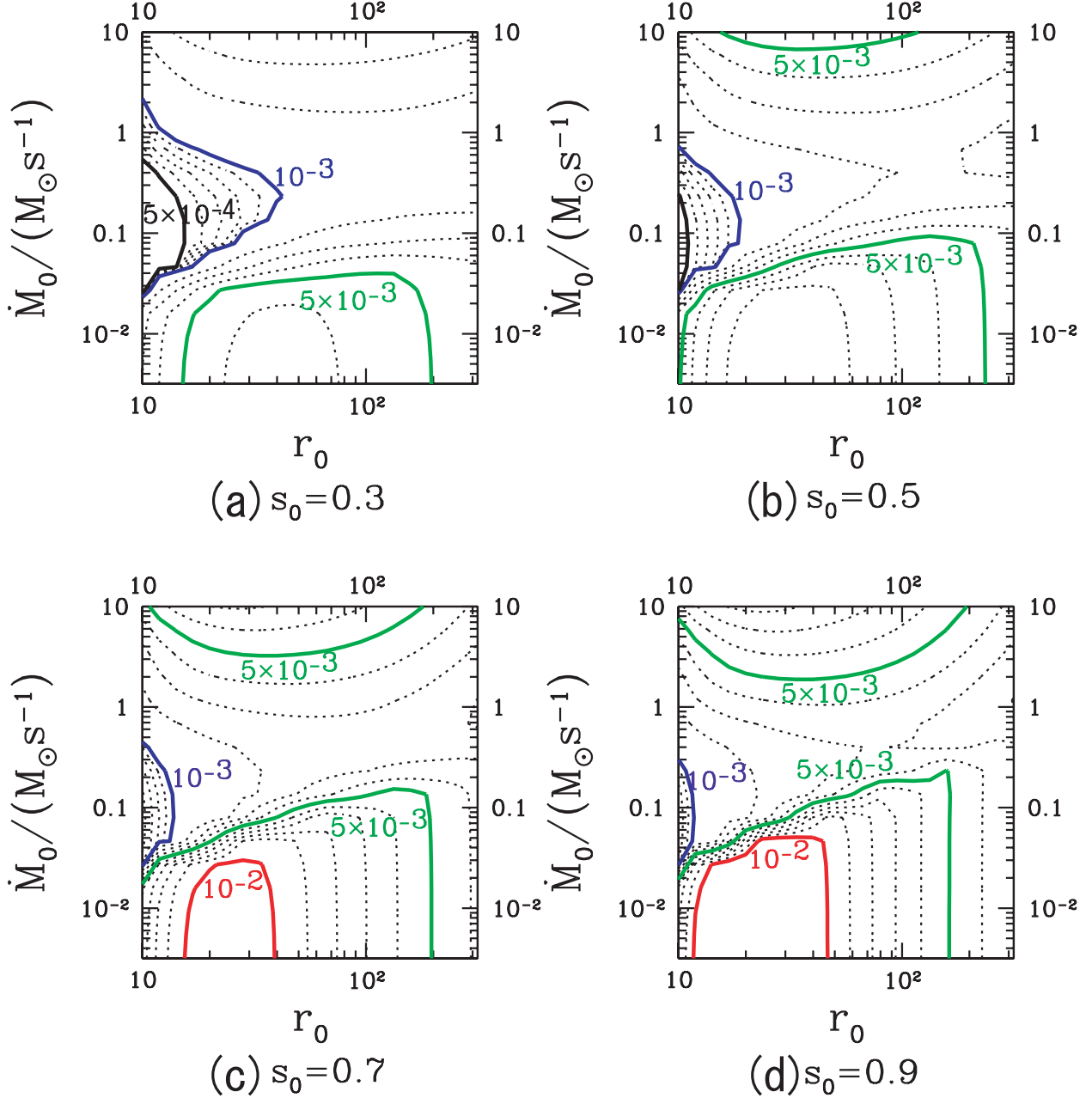


Fig. 8.— (a) Contours of the outflow efficiency $\dot{E}_w/(\xi \dot{M}_0 c^2)$ in the r_0 – \dot{m}_0 plane. Here, the outflow efficiency has been calculated more accurately than in Fig. 7, including the effect of variable advection and using equation (66) for the outflow index $s(R)$ with $s_0 = 0.3$. (b) $s_0 = 0.5$. (c) $s_0 = 0.7$. (d) $s_0 = 0.9$. All results are for $\alpha = 0.1$, $M = 1.4M_\odot$ and $r_{\text{in}} = 7$.

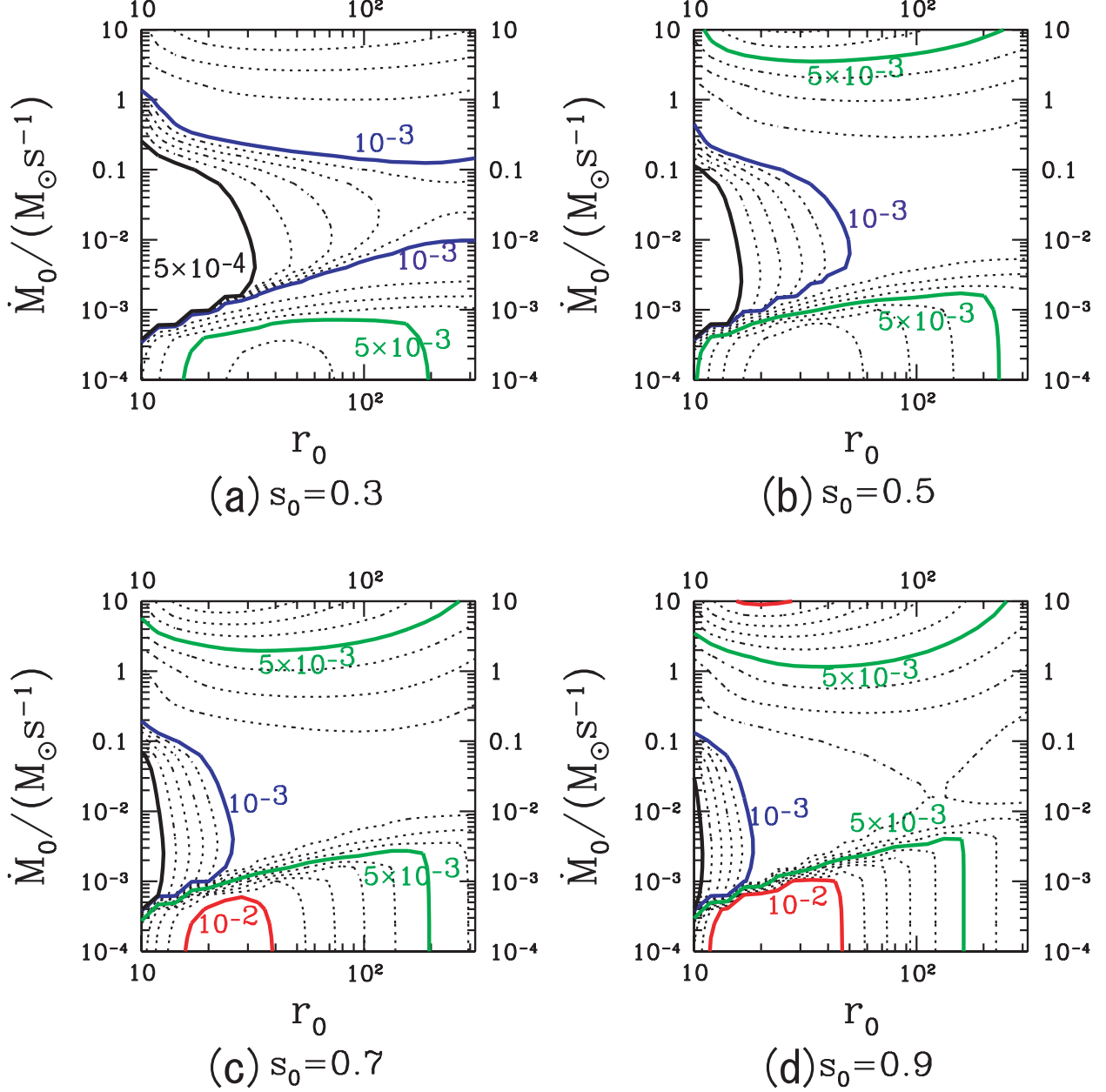


Fig. 9.— Similar to Fig. 8, but for $\alpha = 0.01$. Note that the vertical axis extends over a wider range of \dot{M}_0 .

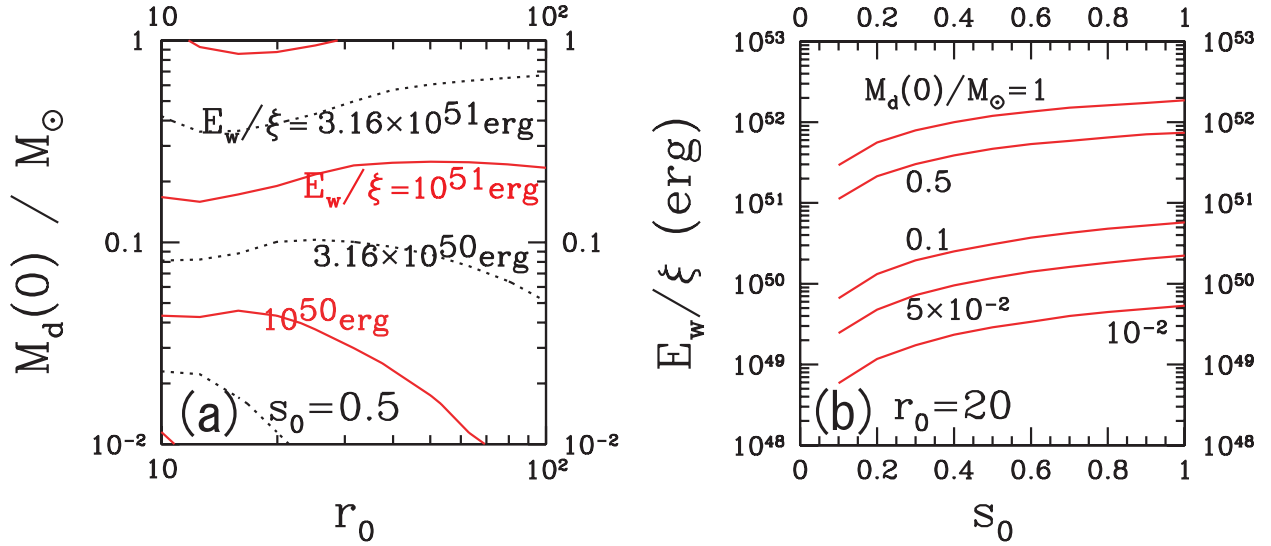


Fig. 10.— (a) Contours of the time-integrated total outflow energy E_w/ξ in the $r_0 - M_d(0)$ plane (where $M_d(0)$ is the initial mass in the disk) for the prompt supernova explosion scenario (§ 3.3). s_0 has been fixed at 0.5. (b) E_w/ξ as a function of s_0 for $r_0 = 20$ for five choices of the initial disk mass: $M_d(0)/M_\odot = 10^{-2}$, 5×10^{-2} , 0.1, 0.5, and 1. All results correspond to $\alpha = 0.1$, $M = 1.4M_\odot$ and $r_{\text{in}} = 7$.

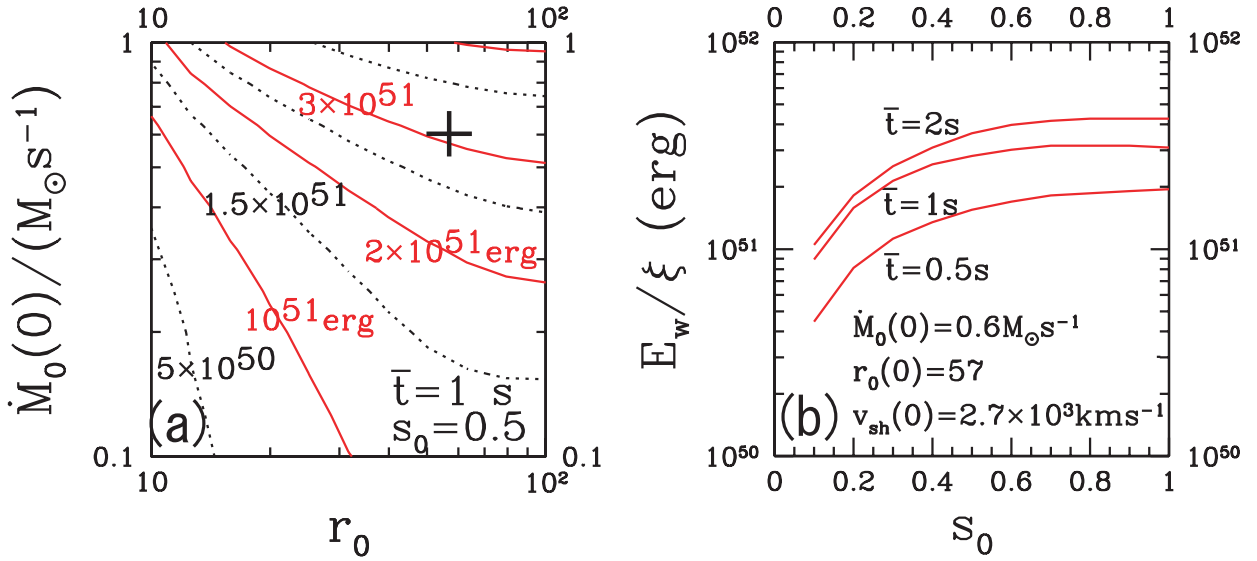


Fig. 11.— (a) Contours of the time-integrated total outflow energy E_w/ξ in the r_0 - \dot{m}_0 plane for the delayed supernova explosion scenario (§ 3.4). The outer edge of the disk is at r_0 which is assumed to be fixed with time. The mass accretion rate is initially \dot{m}_0 and decays exponentially with time with a time constant $\bar{t} = 1$ s. The large cross corresponds to $(r_0, \dot{M}_0) = (57, 0.6 M_\odot \text{s}^{-1})$, a representative example (see § 3.4). (b) E_w/ξ as a function of s_0 for three choices of the decay time constant: $\bar{t} = 2, 1, 0.5$ s. Here, R_0 is assumed to increase with time with a velocity $v_{\text{sh}}(t) = v_{\text{sh}}(0) \exp(-t/\bar{t})$, where $v_{\text{sh}}(0) = 2.7 \times 10^8 \text{ cm s}^{-1}$. All results correspond to $\alpha = 0.1$, $M = 1.4 M_\odot$ and $r_{\text{in}} = 7$.

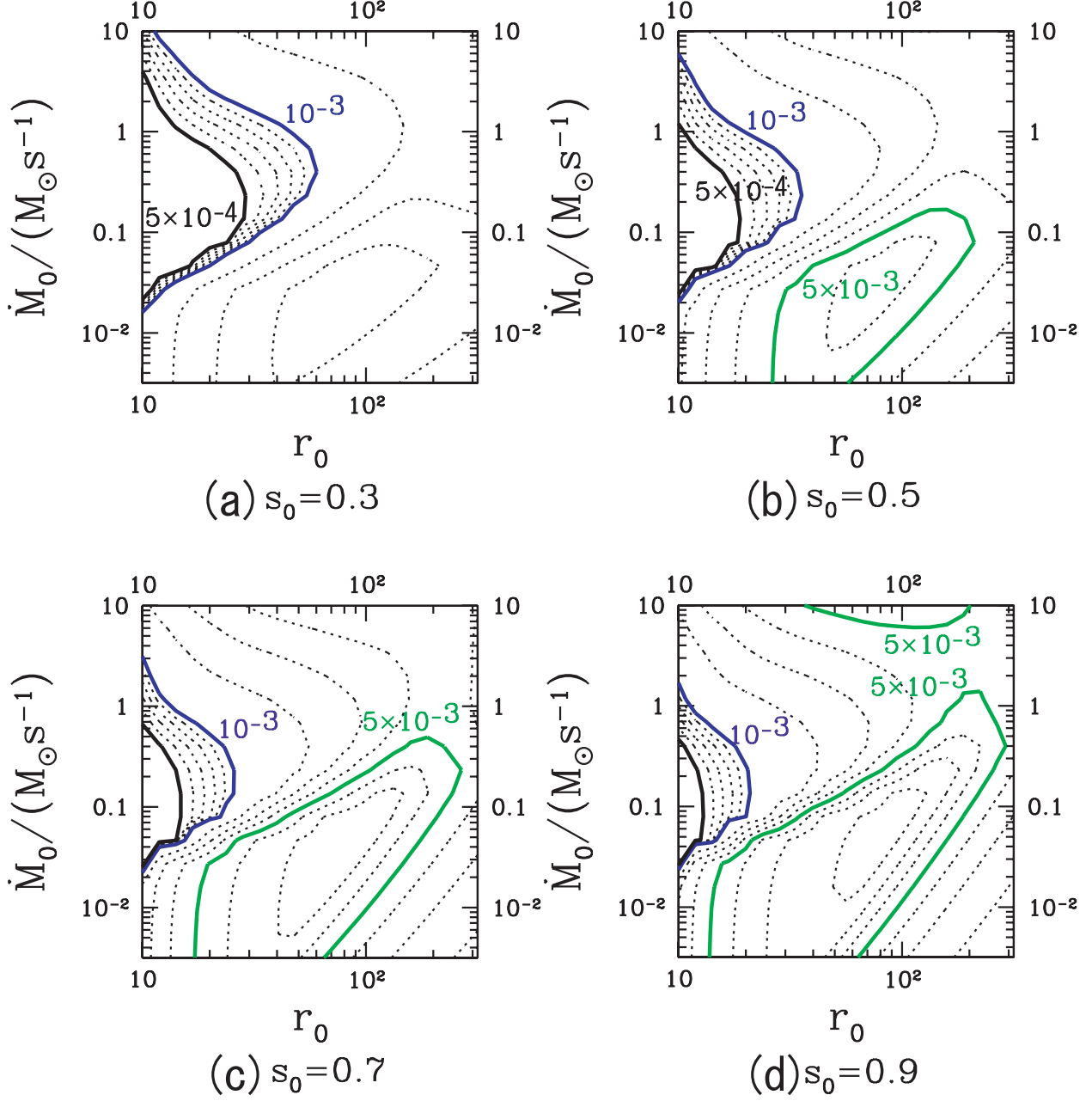


Fig. 12.— (a) Contours of the outflow efficiency $\dot{E}_w/(\xi \dot{M}_0 c^2)$ in the r_0 – \dot{m}_0 plane, including the energy released through recombination of nucleons into nuclei, for $\xi = 0.1$. Compare with Fig. 8 where recombination energy was not included. Contour values in Fig. 8 should be multiplied by 0.1 for the present value of ξ . For this ξ , the recombination energy is seen to be highly significant.

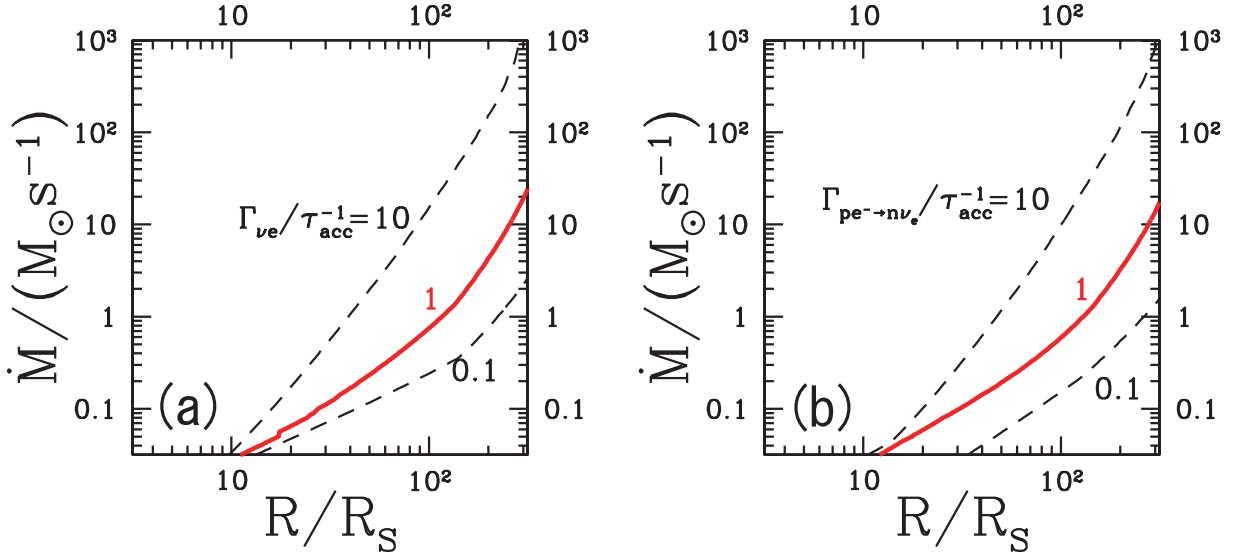


Fig. 13.— (a) Contours of the ratio of the neutrino-electron scattering rate and the accretion rate, $\Gamma_{\nu e}/\tau_{\text{acc}}^{-1}$, in the r - \dot{m} plane. (b) Contours of the ratio of the proton to neutron interconversion rate to the accretion rate, $\Gamma_{pe^- \rightarrow n\nu_e}/\tau_{\text{acc}}^{-1}$. All results correspond to $\alpha = 0.1$ and $M = 1.4M_{\odot}$.

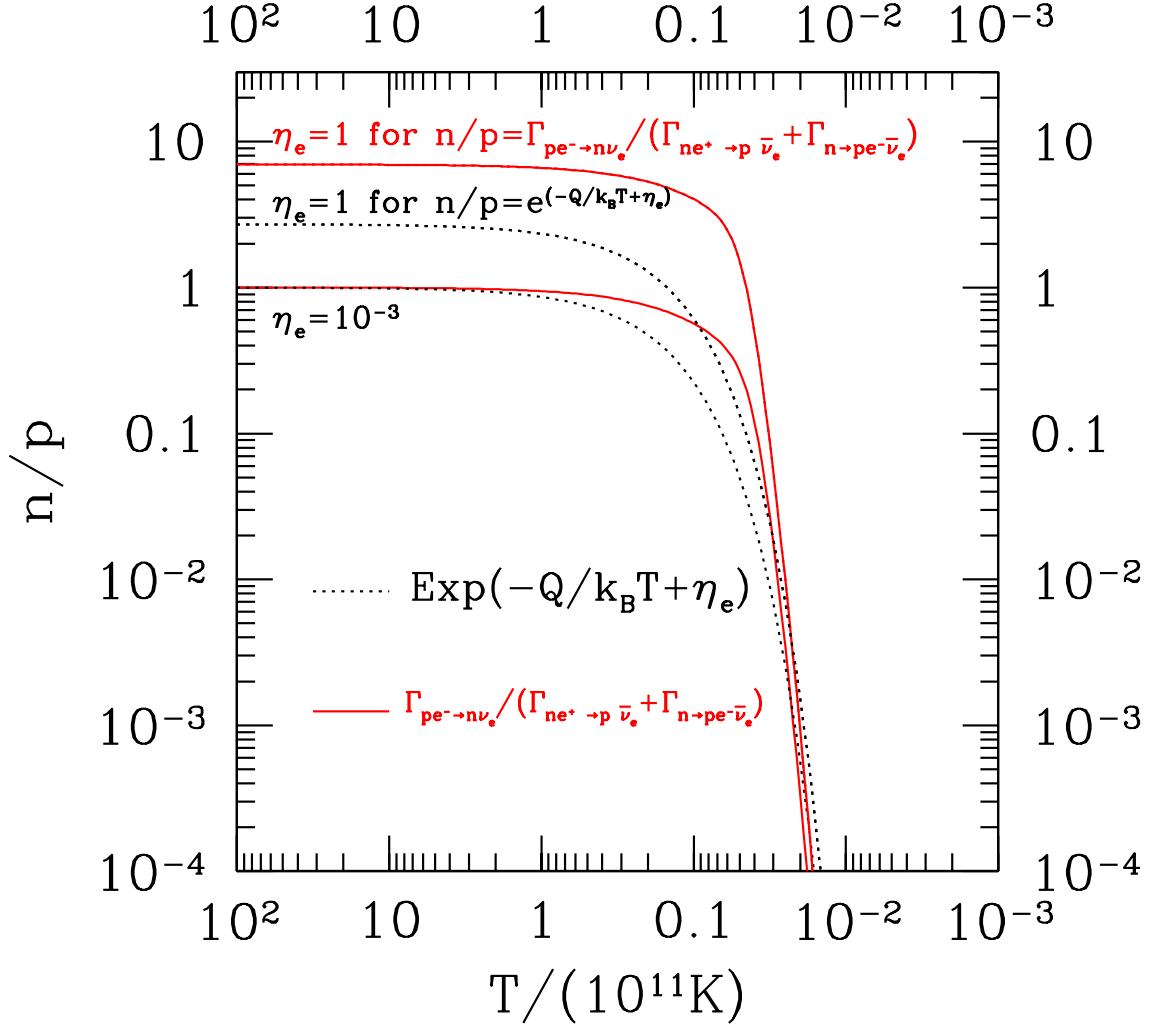


Fig. 14.— Plot of the neutron to proton ratio as a function of the temperature. The dotted lines represent cases in which the neutrinos are completely thermalized and the neutrino-nucleon collisions are important, so that $n/p = \exp(-Q/k_B T + \eta_e)$. The solid lines represent cases in which we omit the neutrino-nucleon collisions, and set $n/p = \Gamma_{pe^- \rightarrow n\nu_e} / (\Gamma_{ne^+ \rightarrow p\bar{\nu}_e} + \Gamma_{n \rightarrow pe^- \bar{\nu}_e})$. The upper (lower) lines correspond to $\eta_e = 1$ ($\eta_e = 10^{-3}$).